On the Interannual Variability of African Easterly Waves and Its Relationship with El Niño–Southern Oscillation

QUINTON A. LAWTON,[a] BROOKE WEISER,[b] AND SHARANYA J. MAJUMDAR[b]

[a] *NSF National Center for Atmospheric Research, Boulder, Colorado*
[b] *Rosenstiel School of Marine, Atmospheric, and Earth Science, University of Miami, Miami, Florida*

(Manuscript received 24 February 2025, in final form 30 June 2025, accepted 22 July 2025)

ABSTRACT: African easterly waves (AEWs) have important impacts on rainfall, drought, and the development of tropical cyclones in the Atlantic basin. However, the interannual variability of AEWs and their near-environmental characteristics are still poorly understood. Using an object-oriented AEW tracker, this study investigates the interannual variability of AEW characteristics and its association with El Niño–Southern Oscillation (ENSO) and Atlantic tropical cyclone activity. The variability of tracked AEW characteristics was found to be largely comparable across two reanalysis datasets, suggesting these fields are reliable indicators of AEW activity. ENSO is shown to impact AEW strength, moisture content, convective activity, and vertical structure on interannual time scales. Supporting this finding is an inverse correlation between these wave attributes and the oceanic Niño index, as well as vertical composites indicating an enhancement of these attributes during La Niña years versus El Niño years. Additionally, the ENSO–AEW relationship is mostly confined to the African continent. It is hypothesized that ENSO influences AEW activity through the modification of regional circulations including the tropical easterly jet, the African easterly jet, and the West African monsoon. These circulations are stronger and displaced during La Niña years, potentially increasing convection in the vicinity of AEWs and enhancing thermodynamic instabilities. Additionally, differences in AEW characteristics between active and inactive Atlantic tropical cyclone years are similar to the differences found between ENSO phases. Overall, these findings demonstrate that the ENSO–AEW relationship is a distinct teleconnection that may have important impacts on local weather and downstream tropical cyclogenesis.

SIGNIFICANCE STATEMENT: African easterly waves (AEWs) are weather systems that can produce extreme rainfall and tropical cyclones. It is not fully known how the attributes of these waves vary on a year-by-year basis. This study shows that El Niño–Southern Oscillation (ENSO), an important climate pattern, has a significant impact on the yearly variability of AEWs. AEWs are stronger, moister, and more convectively active during La Niña versus El Niño. These differences are connected to changes in weather patterns over Africa and hint at a previously unexplored connection between ENSO and tropical cyclone activity through AEWs. Overall, these results provide important insight into the ENSO–AEW relationship that may help improve seasonal forecasts and provide context for understanding climate change.

KEYWORDS: Africa; Atmospheric waves; Tropical cyclones; ENSO; Interannual variability; Tropical variability

1. Introduction

African easterly waves (AEWs) are westward-propagating disturbances that originate over the African continent. During the boreal summer, AEWs are important drivers of rainfall variability in the Sahel region of Africa (Lubis and Jacobi 2015). They are also the primary initial disturbance that precedes tropical cyclone (TC) development in the Atlantic basin (Landsea 1993; Russell et al. 2017). AEW development is driven in part due to barotropic and baroclinic instabilities along the African easterly jet (AEJ) and over the Atlantic (Burpee 1972; Thorncroft and Hoskins 1994; Thorncroft and Blackburn 1999). The AEJ arises from strong meridional temperature gradients between the Saharan Desert and the Sahel, and it is closely connected to other regional atmospheric features like the tropical easterly jet (TEJ) and the West African monsoon (WAM) (Thorncroft and Blackburn 1999; Nicholson 2013).

In addition to dynamical instabilities, moisture and convection play a significant role in the initiation, growth, and propagation of AEWs (Hall et al. 2006; Thorncroft et al. 2008; Berry and Thorncroft 2012; Russell and Aiyyer 2020; Russell et al. 2020; Núñez Ocasio et al. 2020; Vargas Martes et al. 2023; Núñez Ocasio et al. 2024). Convection is a necessary trigger for the growth of thermodynamic instabilities along the AEJ (Hsieh and Cook 2005, 2007; Hall et al. 2006; Thorncroft et al. 2008). Diabatic heating from convective processes also plays an essential role in AEW growth and propagation, in many cases equaling the contributions from adiabatic instabilities

Supplemental information related to this paper is available at the Journals Online website: https://doi.org/10.1175/JCLI-D-25-0113.s1.

Weiser's current affiliation: Moody's Insurance Solutions, New York, New York.

Corresponding author: Quinton A. Lawton, qlawton@ucar.edu

DOI: 10.1175/JCLI-D-25-0113.1

© 2025 American Meteorological Society. This published article is licensed under the terms of the default AMS reuse license. For information regarding reuse of this content and general copyright information, consult the AMS Copyright Policy (www.ametsoc.org/PUBSReuseLicenses).

Unauthenticated | Downloaded 10/23/26 03:43 PM UTC

(Cornforth et al. 2009; Berry and Thorncroft 2012; Tomassini 2018; Russell and Aiyyer 2020; Russell et al. 2020). Additionally, convection serves as a link between other atmospheric circulations and AEW activity. For example, atmospheric Kelvin waves can influence AEW activity through their modulation of convection and moisture (Ventrice and Thorncroft 2013; Lawton et al. 2022; Lawton and Majumdar 2023). The coupling of the WAM to AEW activity is also thought to occur in part through convection, due to the strong influence of monsoonal flow on moist convection over Africa (Sultan et al. 2003; Sylla et al. 2010; Nicholson 2013). It has been shown that the strength of this monsoonal flow can influence the phase locking of convection to AEWs, affecting wave growth and their favorability to undergo TC genesis (Núñez Ocasio et al. 2021, 2024).

Given the known relationships between atmospheric circulations, convection, and AEWs, it has been suspected that changes to these large-scale environmental factors could influence the interannual variability of AEWs. For example, the Atlantic Niño has been implicated in enhancing AEW activity and thus the likelihood of TC formation (Kim et al. 2023). Similarly, the Atlantic meridional mode (AMM) modulates temperature gradients in the tropical Atlantic on interannual-to-decadal time scales, impacting TC activity and potentially their AEW seeds (e.g., Patricola et al. 2014). However, while there has been a plethora of research documenting the mean climatology of AEWs and their intraseasonal variability (Leroux and Hall 2009; Hopsch et al. 2010; Alaka and Maloney 2012, 2014; Brammer and Thorncroft 2015; Belanger et al. 2016; Lawton et al. 2022; Bercos-Hickey and Patricola 2024), less work has been focused on the interannual variability of wave characteristics and behavior. Most existing work has either focused on this variability in the context of TC genesis (Thorncroft and Hodges 2001), analyzed AEWs in specific oceanic or coastline regions (Dominguez et al. 2020), or identified AEW activity using indirect proxies rather than via tracked AEW centers for which characteristics of the waves can be directly quantified (e.g., Ruti and Dell'Aquila 2010; Spinks and Lin 2015).

Nevertheless, a few studies have found an association between interannual AEW variability and El Niño–Southern Oscillation (ENSO). Ruti and Dell'Aquila (2010) used 2–6-day bandpass-filtered meridional winds to demonstrate a correlation between ENSO phase and AEW activity near the Guinean coast, with cold ENSO events (La Niña) associated with enhanced wave activity. They argued that this behavior could be explained by the influence of ENSO on the global east–west circulation pattern in the upper troposphere and its modification of subsidence over West Africa. Spinks and Lin (2015) found a similar relationship between ENSO phase and AEW activity using temporal averages of unfiltered curvature vorticity. They suggested that ENSO could influence east–west differential heating over Africa, which maintains the Saharan and Arabian highs and thus the meridional temperature gradients important for the AEJ and TEJ. More recently, Didi et al. (2023) demonstrated that La Niña years are associated with enhanced West African rainfall, a stronger TEJ and WAM, and a poleward shift in the position of the AEJ. While they did not directly investigate propagating waves, their finding hints at the possibility of ENSO-driven changes to African rainfall and atmospheric circulations influencing AEW activity through diabatic heating and thermodynamic growth processes. In fact, a potential ENSO–AEW relationship may not be confined to the African continent; Dominguez et al. (2020) showed that easterly waves contribute more to rainfall over northern South America during La Niña years as compared to neutral and El Niño years.

One reason a potential ENSO–AEW connection is intriguing is due to the importance of AEWs in seeding TC activity in the Atlantic Ocean (Russell et al. 2017). ENSO has already been separately implicated in modifying the seasonal favorability of TC development in the Atlantic basin (Shapiro 1987; Gray 1984; Landsea and Gray 1992). On interannual time scales, the positive phase (El Niño) of ENSO is associated with a significant increase in vertical wind shear over large parts of the main development region (MDR), particularly in the Caribbean Sea (Shapiro 1987; Aiyyer and Thorncroft 2006). El Niño is also associated with a basinwide decrease in midlevel relative humidity (Camargo et al. 2007). As a result, TC activity in the Atlantic is generally suppressed during El Niño years. Conversely, there is reduced vertical wind shear and enhanced TC activity during La Niña years. While the known ENSO teleconnection to TCs through basinwide vertical wind shear and moisture is well studied, less is known about the effects of ENSO on the AEW disturbances that form into TCs. If ENSO did make AEWs structurally more favorable to undergo TC genesis, it would represent a separate teleconnection between ENSO and TC activity from that which has been previously established. Regardless of the implications for TC activity, changes to AEW characteristics could have important implications for flooding and drought in the Sahel region.

We argue that object-based AEW tracking presents an opportunity to better elucidate the interannual variability of AEW characteristics and their relationship with ENSO and TC activity. A significant drawback of previous research has been its utilization of indirect measures of AEW activity and little focus on important wave characteristics, such as their vertical structure or surrounding environmental fields (Ruti and Dell'Aquila 2010; Spinks and Lin 2015). While these proxies can be informative, they do not provide a complete picture of wave attributes and behavior and can often conflate AEWs with other transient disturbances. This is especially important given widespread evidence that wave-to-wave variability in AEW attributes, like their vertical structure, moisture content, and convective activity, has significant ramifications on their impacts and the favorability of TC genesis (Agudelo et al. 2011; Brammer and Thorncroft 2015; Brammer and Thorncroft 2017; Núñez Ocasio et al. 2021; Lawton and Majumdar 2023). In contrast to the use of indirect wave proxies, the use of wave tracking allows such characteristics to be better quantified and has been used for other phenomena, like mesoscale convective systems (e.g., Prein et al. 2024). Such work also presents an opportunity to validate object-based AEW tracking metrics across multiple reanalysis datasets.

In this paper, we investigate the interannual variability of AEW characteristics and their association with both ENSO

Unauthenticated | Downloaded 10/23/26 03:43 PM UTC

and Atlantic TC activity using a 40+ year dataset of tracked easterly wave objects in two reanalysis datasets. Wave tracking allows us to more directly quantify wave characteristics and their seasonal statistics. We first describe the climatology and variability of AEWs and explore their consistency between reanalyses (section 3). We then examine how the interannual variability of wave characteristics is associated with ENSO and TC activity (section 4). Finally, we relate these findings to regional atmospheric circulations in Africa (section 5) and describe the implications of these results for our understanding of ENSO–TC teleconnections (section 6).

2. Materials and methods

a. Data

We utilize two sets of reanalysis data for AEW identification and environmental analysis: the European Centre for Medium-Range Weather Forecasts (ECMWF) ERA5 dataset (Hersbach et al. 2020) and NASA's MERRA-2 dataset (Gelaro et al. 2017). Both reanalyses are obtained with a 6-hourly temporal resolution from 1981 through 2023 and are conservatively remapped to a 1° × 1° grid. We primarily analyze the months June–October, which encompass the peak of AEW activity and their contributions to precipitation variability (Burpee 1972; Thorncroft and Hodges 2001; Fig. 14a in Lubis and Jacobi 2015). Satellite brightness temperature T_b data are obtained from the NOAA GridSat-B1 dataset (Knapp et al. 2011). For efficiency, T_b data are also conservatively remapped to a 1° × 1° grid. Because this study primarily focuses on AEW-relative averages and statistics, the lower spatial resolution is unlikely to influence overall results. However, we acknowledge that reanalyses may contain uncertainties in data-sparse regions. While no comparable observational dataset is available to fully validate reanalysis AEWs, this caveat motivates our use of multiple state-of-the-art reanalysis datasets and is taken into account in our interpretation of results.

To build AEW-relative composites of environmental fields, climatological anomalies are computed using the first four harmonics of the mean annual cycle. To account for the diurnal cycle, these four harmonics are removed separately for each six-hour period (0000, 0600, 1200, and 1800 UTC). Environmental variables are then averaged in a 10° × 10° box surrounding the AEW center. This box size is a compromise between including the most important aspects of the AEWs while excluding external phenomena, and it is close in size to the 600-km radial averages used in previous studies of AEW characteristics (e.g., Brammer and Thorncroft 2015; Lawton et al. 2022).

b. Easterly wave identification

We utilize the tracker described by Lawton et al. (2022), in which AEWs are identified using radially averaged curvature vorticity (CV) fields at 700 hPa. This tracking algorithm is now available publicly as a Python module named "QTrack"; the tracks used in this study were generated using version 0.0.4 of this module (Lawton 2024a). Vorticity fields have frequently been used by AEW trackers to identify AEWs (Bain et al. 2014; Brammer and Thorncroft 2015; Hollis et al. 2024; Fischer et al. 2024). However, QTrack differs from other wave trackers in that its algorithm adapts to the AEW's location and incorporates several postprocessing steps to connect and validate AEW tracks. QTrack is especially useful at identifying AEWs over the African continent and eastern Atlantic, and it has been successfully used in reanalysis and modeling studies (e.g., Lawton et al. 2022; Núñez Ocasio et al. 2024).

While QTrack v0.0.4 is very similar to the tracker developed by Lawton et al. (2022), there are a few key changes. Easterly waves can now initiate and propagate in both the Atlantic and Pacific basins, and the nondivergent wind calculation step is skipped. Otherwise, the core algorithm and process are unchanged. As in previous studies utilizing this tracker, easterly waves are classified as "developing" waves if they are located within 500 km of a TC in the HURDAT database at the time of TC genesis (Landsea and Franklin 2013). Developing waves consist of 14% and 17% of the tracked waves in ERA5 and MERRA-2, respectively. We also note that initiating waves requires exceeding a CV threshold of $2 \times 10^{-6}\ s^{-1}$, and the continuation of existing waves requires exceeding a CV threshold of $1 \times 10^{-7}\ s^{-1}$. Of the waves tracked for this analysis, roughly 65% originated in the Atlantic and 35% originated in the Pacific. Additional data, Python scripts, and more information can be found in a GitHub repository (Lawton 2024a).

It is worth pointing out that many of the waves identified by QTrack, especially in the open Atlantic and Pacific, are not necessarily African easterly waves. Indeed, AEWs have dynamics and characteristics that can differ from easterly waves in the Pacific and other basins (Vargas Martes et al. 2023; Hollis et al. 2024). While our focus here is on AEWs over Africa and the Atlantic, the climatology and statistics of easterly waves over the Pacific are also included for completeness. For simplicity, we refer to waves identified over the Atlantic and African continents as AEWs and those over the Pacific more generally as easterly waves. However, we caution that many waves in the open Atlantic and Caribbean Sea may not have originated as an AEW and could differ in dynamics and behavior. In this study, we compute separate statistics for waves located over the Pacific basin and those located over the Atlantic basin.

c. Quantifying ENSO and TC activity

This study uses an approach that compares AEWs and their characteristics across multiple groupings of years. To do so, we classify AEW seasons that were concurrent with an ENSO phase, significantly low TC activity, or significantly high TC activity. ENSO is defined using the oceanic Niño index (ONI), which is computed using a three-month running mean of sea surface temperature anomalies in the Niño-3.4 region (NOAA 2009). We chose the ONI value for each year with a running mean across the months of July–September, overlapping the seasonal peak of AEW activity. We then follow the NOAA threshold of ±0.5°C in defining warm and cold ENSO events, with the resulting year categorizations presented in the top

Unauthenticated | Downloaded 10/23/26 03:43 PM UTC

TABLE 1. Categorization of years based on ENSO phase and seasons of reduced and enhanced Atlantic TC activity. Bolded years overlap that of another category, either La Niña years with active TC years or El Niño years with inactive TC years.

Category	Primary threshold (0.5 ONI, 25% TC)
La Niña years	**1988**, **1995**, **1998**, 1999, **2000**, 2007, **2010**, 2011, **2016**, **2020**, 2021, 2022
El Niño years	**1982**, **1986**, 1987, 1991, 1994, **1997**, **2002**, 2004, 2006, 2009, 2015, 2023
Active TC years	**1988**, 1989, **1995**, **1998**, **2000**, **2010**, 2012, **2016**, **2020**, 2023
Inactive TC years	1983, 1992, **1982**, 1984, 1985, **1986**, 1993, **1997**, **2002**, 2022

two rows of Table 1. Neutral years are those classified as neither El Niño nor La Niña. We also generated results using an ONI threshold that was more (±0.75°C) and less (±0.25°C) restrictive; this sensitivity testing did not significantly alter the results and conclusions presented here.

TC activity is defined as the number of TC genesis events that takes place over the eastern Atlantic (east of 60°W) during the months of June–October and that are associated with a tracked easterly wave. This region is chosen because most TC genesis events in this area are primarily seeded by AEWs (Russell et al. 2017). The top and bottom 25% of yearly seasonal TC counts are then used to define "active" and "inactive" TC years, shown in the bottom two rows of Table 1. As for the ENSO years, results generated using more (15%) and less (35%) restrictive thresholds were also similar. More information about these threshold sensitivity tests can be found in the online supplemental materials (Table S1).

Due to the well-known teleconnection between ENSO and Atlantic TC activity, more than half of the active TC years overlap that of the La Niña years (Table 1). There is a similar overlap between inactive TC and El Niño years. As a result, the ENSO and TC activity year samples are not entirely independent of one another, and thus, it is important not to overinterpret a causal relationship between the two. We also note that many of the active TC years are concentrated in more recent years, perhaps due to the increase in recorded Atlantic TC formation over the past few decades (Vecchi et al. 2021).

3. Variability of African easterly waves

a. *Wave climatology*

We first examine the climatology of tracked AEWs in ERA5 and MERRA-2 data. As discussed previously, the version of QTrack used in this study slightly differs from that used by Lawton et al. (2022), primarily in that it is able to propagate easterly waves in both the Atlantic and Pacific basins. This is evidenced by the track and genesis density plots shown in Fig. 1. Overall, these track and genesis densities are similar in pattern across both reanalysis datasets, albeit with the east and central Pacific having slightly higher track densities in MERRA-2 than in ERA5 (Figs. 1a,c).

As has been shown in previous climatologies (Brammer and Thorncroft 2015; Lawton et al. 2022; Hollis et al. 2024), AEWs that propagate into the Atlantic basin typically originate along the AEJ in West Africa and the eastern Atlantic (Figs. 1a–d). In the Pacific, there is a belt of easterly wave activity extending from the Central American coast to the international date line. Many of these waves are first tracked around 100°–80°W. The generation of tracked waves in this region is probably a combination of new easterly waves formed by genesis dynamics over South and Central America (Torres et al. 2021; Zhou and Maloney 2025), as well as the reidentification of AEWs that become too weak for the tracker to capture through the Caribbean. The cause of the localized region of high genesis densities located around 80° and 60°W is unclear, but we note that known deficiencies in AEW tracking due to enhanced background curvature

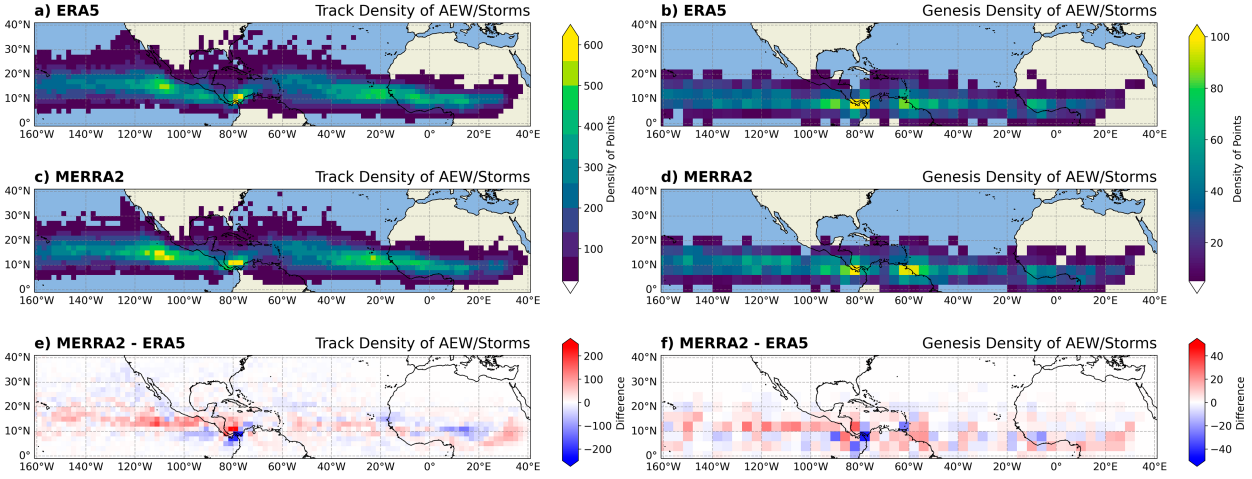


FIG. 1. Track and genesis densities of all tracked AEWs, including developing AEWs before and after TC genesis, using (a),(b) ERA5 and (c),(d) MERRA-2 data for the years 1981–2023 and months July–October. The 2° × 2° bins are used for track densities, and 4° × 4° bins are used for genesis densities. (e),(f) MERRA-2–ERA5 differences in the climatology of track and genesis density.

Unauthenticated | Downloaded 10/23/26 03:43 PM UTC

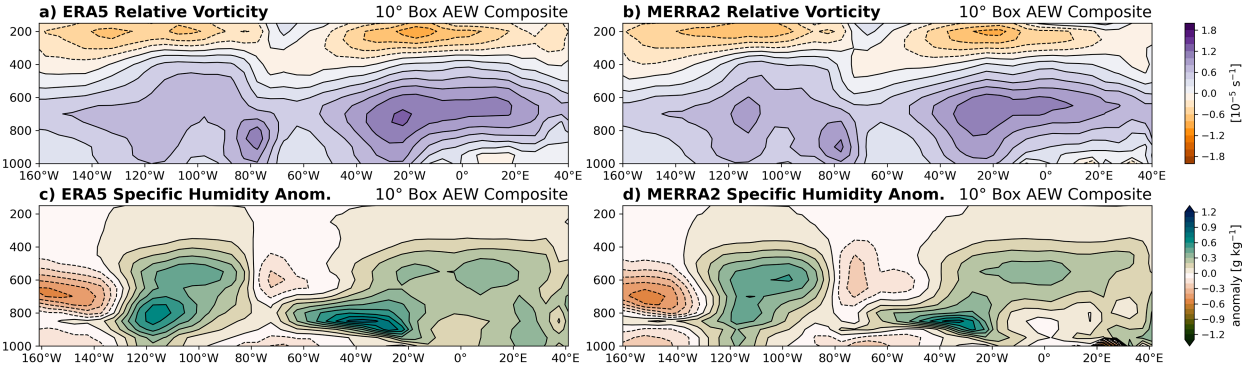


FIG. 2. (a),(b) Longitude climatology of relative vorticity and (c),(d) specific humidity anomalies averaged in a 10° × 10° box surrounding easterly waves tracked at 700 hPa. These AEW-relative averages are composited every 5° of longitude to build a longitudinal climatology. Both developing and nondeveloping AEWs are included, but time steps at and after TC genesis are excluded from the composite. (left) Composites using ERA5 data and tracks are compared to (right) those made using MERRA-2.

vorticity over South America may impact this region.[1] Meanwhile, differences in wave track and genesis densities (Figs. 1e,f) illustrate elevated values in MERRA-2 for both basins. MERRA-2 also has larger densities of formation events in eastern Africa (~20°–30°W) and a genesis region near Central America that is shifted northward.

The average vertical structure of easterly waves also has a distinct longitudinal pattern. As shown in Figs. 2a and 2b, AEWs have a relative vorticity signature that is maximized at midlevels (between 750 and 600 hPa) while transiting the African continent. When AEWs reach the African coastline, their average relative vorticity increases and deepens to lower levels. In contrast, easterly waves over the open Atlantic and Pacific basins are generally weaker and less vertically extensive. A similar pattern also exists for AEW-relative specific humidity anomalies (Figs. 2c,d). When AEWs are over the African continent, their moisture anomalies are generally confined to midlevels. In contrast, waves near the African coastline and over the eastern Atlantic have larger specific humidity anomalies extending to lower levels (925–800 hPa). Overall, these longitudinal climatologies are quite similar for waves in ERA5 and MERRA-2 data and mirror previous research into AEW characteristics (Janiga and Thorncroft 2013; Brammer and Thorncroft 2015; Russell and Aiyyer 2020; Lawton et al. 2022).

b. *Variability*

We now shift to an analysis of the interannual variability of AEW characteristics and behavior. Focus is placed on nondeveloping AEWs to limit biases that could be introduced from developing AEWs, though the trends for developing AEWs were found to be qualitatively similar (not shown). Figure 3 compares total Atlantic AEW count, average AEW strength, and average AEW latitude at the African coastline. These are displayed alongside metrics for ENSO activity (ONI; left column) and TC activity (TC count; right column), which will be discussed in more detail in section 4. Compared with ERA5, the MERRA-2 reanalysis has markedly more Atlantic AEWs than in the ERA5 dataset, especially in the time period from 1980 to 2005. In fact, AEW counts in the Atlantic are not significantly correlated between ERA5 and MERRA-2 data at all, with a remarkably small R value of 0.20 (Table 2). This differs from the eastern Pacific basin, where easterly wave count is still significantly correlated with an R value exceeding 0.50 (Table 2; Fig. S3). The seasonal average of AEW strength, defined as the average 700-hPa CV within 600 km, also trends slightly higher for MERRA-2. Overall, AEW strength and coastline latitude are still highly correlated between the reanalysis datasets in both the Atlantic (Fig. 1 and Table 2) and Pacific basins (Fig. S3, Table 2), and the number of captured developing waves is strongly tied to basinwide TC activity (Table 2).

Annual averages of environmental characteristics surrounding each wave (10° × 10° box), including relative vorticity, specific humidity, and GridSat-B1 T_b, are compared in Fig. 4. In general, there is a high correlation between midlevel AEW characteristics in ERA5 and MERRA-2 data. Results are also correlated for low-level wave characteristics and when using convective coverage instead of average T_b as a proxy for convective activity (not shown). Of particular note is that the midlevel vorticity surrounding AEWs appears to be more consistent between datasets than the AEW strength metric used in Fig. 3, with a much higher interannual correlation (R of 0.68 vs 0.48) and no clear systematic bias (Fig. 4; Table 2). Results are similar for the Pacific basin, with one exception: The correlation between midlevel relative vorticity in ERA5 and MERRA-2 is weak and nonsignificant for Pacific easterly waves (Table 2). This may be because Pacific easterly waves can have circulations that are located closer to the surface than AEWs (e.g., more easterly waves are identified at 850 hPa than 700 hPa in Hollis et al. 2024; see their Fig. 2), with weaker relative vorticity anomalies from 400 to 600 hPa (Figs. 2a,b). In line with this, using 850–700-hPa average relative vorticity yields a cross-reanalysis correlation that is relatively strong (R of 0.51) and significant ($p < 0.01$).

[1] Readers interested in AEW tracking in the Caribbean are encouraged to read a recent publication by Downs et al. (2025) contextualizing this research problem.

Unauthenticated | Downloaded 10/23/26 03:43 PM UTC

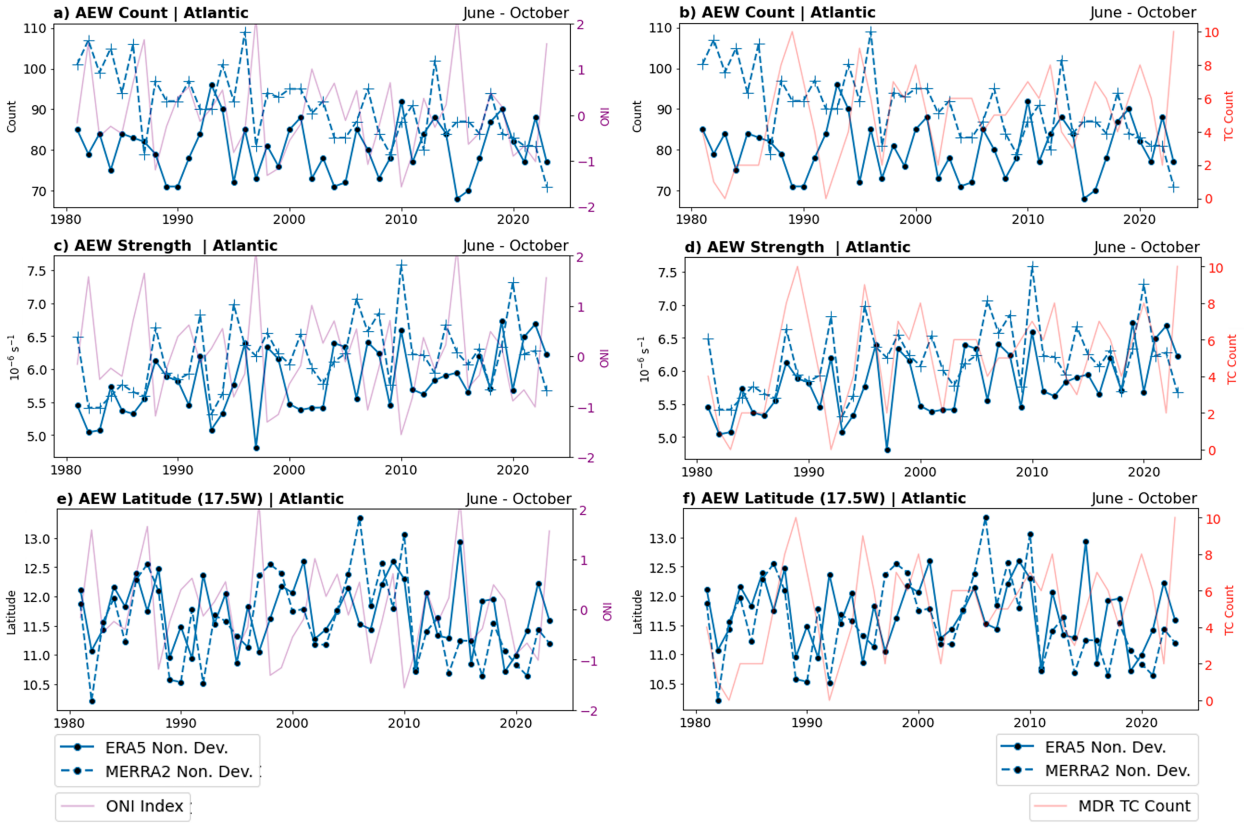


FIG. 3. Subpanels showing each year's (a),(b) total AEW count, (c),(d) average AEW strength (average 700-hPa vorticity within 600-km radius), and (e),(f) average coastline AEW latitude (averaged tracked latitude for AEWs as they exist coastline near 17.5°W) for the Atlantic basin. Data from nondeveloping AEWs tracked in ERA5 (solid blue line) and MERRA-2 (dashed blue line) are included as separate lines and are identical for both panels in each row. (left) The June–September ONI (purple line) are plotted for comparison; (right) yearly Atlantic TC counts (red) are plotted for comparison.

Another observation is that the average AEW strength (Figs. 3c,d), AEW-relative vorticity (Figs. 4c,d), and AEW specific humidity (Figs. 4a,b) in the Atlantic basin all appear to trend higher with time. In ERA5 data, there are statistically significant differences in average AEW strength and 700–400-hPa specific humidity between the first half (1981–2002) and the second half (2003–23) of the climatology (Fig. S4). These differences are not significant using MERRA-2 data, limiting our confidence in these trends. We also note that the basinwide (0°–20°N; 40°W–40°E) variability in humidity and relative vorticity mirrors that of AEWs, making it hard to determine if AEWs are simply propagating in a changed background environment or are contributing to these basinwide changes (Fig. S5). Nevertheless, recent research has indicated there could be changes to AEW activity in future warming scenarios, with the direction and magnitude of these changes varying by study (Akinsanola et al. 2025; Hannah and Aiyyer 2017; Skinner and Diffenbaugh 2014, so forth). While evaluating observed AEW climate trends is outside the scope of this study, our findings motivate future work to clarify the relationship between AEWs and climate change in the context of future projections.

TABLE 2. Pearson's correlation coefficients and associated p values comparing basic easterly wave characteristics in ERA5 vs MERRA-2 data, separated by basin. Correlations are bolded if they have a p value below 0.05. Captured TC genesis indicates the correlation between basinwide TC counts and the number of developing waves captured by the easterly wave tracker.

	Atlantic		Pacific	
ERA5 vs. MERRA-2 correlations	R	p value	R	p value
Easterly wave/AEW count	0.20	0.19	**0.53**	**<0.01**
Easterly wave/AEW strength	**0.48**	**<0.01**	**0.37**	**0.01**
Wave latitude at 17.5°W/112.5°W	**0.36**	**0.02**	**0.40**	**<0.01**
Captured TC genesis	**0.65**	**<0.01**	**0.60**	**<0.01**
AEW 400–700-hPa average q_v	**0.80**	**<0.01**	**0.87**	**<0.01**
AEW 400–700-hPa average vorticity	**0.68**	**<0.01**	0.17	0.27
AEW average T_b	**0.76**	**<0.01**	**0.81**	**<0.01**

Of the metrics explored here, total AEW count and average AEW CV strength (Fig. 3) had the weakest correlation between the ERA5 and MERRA-2 datasets. This casts some doubt on the use of these metrics as a reliable measure of AEW activity and has implications for the identification of interannual extremes. To highlight this, Table 3 lists the five top and bottom AEW seasons for each reanalysis as defined via

Unauthenticated | Downloaded 10/23/26 03:43 PM UTC

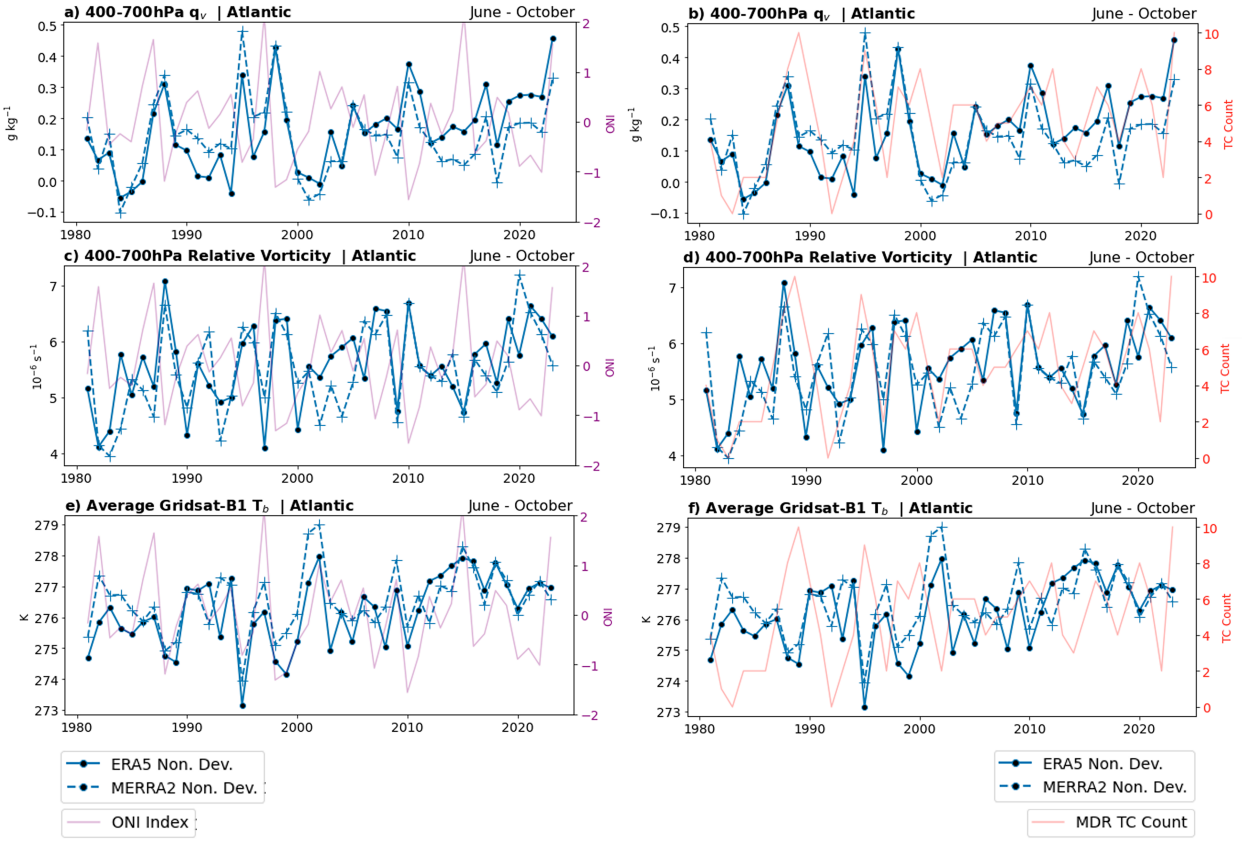


FIG. 4. As in Fig. 3, but for (a),(b) the 400–700-hPa average specific humidity q_v, (c),(d) the 400–700-hPa average relative vorticity, and average brightness temperature T_b in a $10^\circ \times 10^\circ$ box surrounding AEW centers.

various measures of AEW activity, including average wave strength and total wave count. In general, these extreme years vary wildly between the ERA5 and MERRA-2 datasets. For example, not a single top five or bottom 5 years defined by ERA5 AEW count appears in the corresponding list using MERRA-2 data. Using average AEW strength does result in more overlapping years. Nevertheless, it is clear that the choice of reanalysis dataset affects our ability to rank and categorize extremes in seasonal AEW activity.

We consolidate AEW strength and seasonal count into a single metric by integrating AEW strength in time during each season, a metric we refer to as "cumulative strength." This cumulative strength is averaged over all tracked years and shown as a function of day of year for the Atlantic basin in Fig. 5. The average time derivative of cumulative strength is also displayed. Figure 5 makes clear that by the end of the season, average AEW cumulative strength in the Atlantic is higher in MERRA-2 than in ERA5. This is contributed to by

TABLE 3. The top and bottom 5 years of AEW activity in the Atlantic defined by either the yearly average cumulative AEW strength, yearly average AEW strength (CV), or the yearly total AEW count. Higher rows indicate more extreme years; for example, the first top 5 years have the largest value, whereas the first bottom 5 years have the smallest value. These are subset by the reanalysis dataset. Years are bolded if they exist in the corresponding list for the other reanalysis dataset (e.g., 2010 appears in both the ERA5 and MERRA-2 top 5 years as defined by average AEW strength).

Sorted by cumulative strength				Sorted by average strength				Sorted by total count			
ERA5		MERRA-2		ERA5		MERRA-2		ERA5		MERRA-2	
Top	Bottom	Top	Bottom	Top	Bottom	Top	Bottom	Top	Bottom	Top	Bottom
2022	1983	2010	1984	2019	1997	**2010**	**1993**	1993	2015	1996	2023
1996	1997	1992	2023	2022	**1982**	2020	**1983**	2010	2016	1982	2009
2021	1993	2014	**1994**	**2010**	**1983**	2006	**1982**	2019	1989	1986	1987
2007	**1994**	2006	2018	2021	**1993**	1995	1987	1994	1990	1984	2012
2019	2012	**2021**	1990	2007	1986	2008	1984	2001	2004	2013	1997

Unauthenticated | Downloaded 10/23/26 03:43 PM UTC

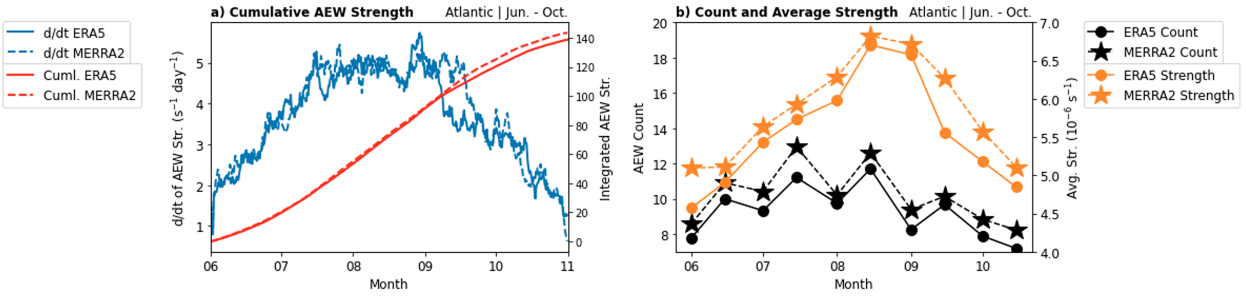


FIG. 5. (a) Cumulative AEW strength (red lines), defined as the integral of AEW strength (CV), and the average time derivative of cumulative AEW strength (blue lines). Data are averaged across all AEW seasons (1981–2023) for the Atlantic basin. Dashed lines are used for MERRA-2 data and solid lines for ERA5 data. (b) Average wave count (black lines) and strength (orange) computed every half-month from June to October.

the higher wave counts and average AEW strength seen for MERRA-2 tracks (Figs. 3a–d). Meanwhile, the time derivative (blue line in Fig. 5) illustrates that the largest contributions to cumulative strength occur from mid-July until the beginning of September. It is at the end of this time period where ERA5 and MERRA-2 diverge significantly. MERRA-2 data depict the most active period of AEW activity extending further into September than ERA5 data, largely a result of differences in average AEW strength in the month of September (Fig. 5b). This disagreement between reanalyses is also evident when cumulative strength is used to determine extremes in AEW seasons (Table 3).

Additional analysis reveals that reanalysis differences in wave count and strength during September are most prominent in earlier years and are mostly confined to nondeveloping AEWs (1981–2002; Fig. S6). Waves in MERRA-2 data also exhibit overall shorter lifetimes and increased track density over central and eastern Africa (Figs. 1e,f; Fig. S7). The cause of these discrepancies is not immediately clear. However, there exist significant differences in the ERA5 and MERRA-2 data assimilation systems and underlying atmospheric models that may contribute to these early year deviations. For example, ERA5 uses 4D-Var data assimilation with a 41-km/137-level atmospheric model, whereas MERRA-2 uses 3D-Var and a coarser model with reduced vertical levels. It is possible these differences could alter the representation of the atmosphere in data-sparse tropical regions and earlier time periods with reduced observations. We also suspect that such disagreements may manifest most prominently in the AEW count due to our use of a fixed CV threshold for wave initialization across both datasets (see section 2a). While this reasoning remains just one hypothesis, it is supported by the shorter MERRA-2 wave lifetimes and increased wave density over typical genesis regions (like eastern Africa), suggesting that count differences may be driven by marginal AEWs that are especially sensitive to the initial wave threshold. Separately, there is some evidence that MERRA-2 could overmoisten the tropics, which could also impact the representation of AEWs (Johnston et al. 2021).

This analysis demonstrates that some measures of AEW climatology and interannual variability are more comparable between ERA5 and MERRA-2 than others. In general, averages of environmental variables surrounding AEWs are relatively consistent between the reanalyses. In contrast, seasonal AEW counts and statistics attempting to quantify years of extreme AEW activity vary significantly between these datasets, especially in earlier years (1981–2002). It is impossible to verify which of these reanalysis depictions is the "correct" answer. However, this finding suggests that these variables may not be dependable indicators of AEW activity. Such metrics, especially easterly wave count, will be deemphasized in later sections, and we recommend users of object-oriented trackers to interpret AEW count and yearly extremes with caution.

4. Relationship with ENSO and TC activity

a. *Basic AEW attributes*

We now analyze the association between measures of ENSO, TC activity, and characteristics of AEW behavior in the Atlantic basin. In the last section, July–September ONI and seasonal Atlantic TC counts were displayed alongside the interannual variability of AEW attributes (Figs. 3 and 4, Figs. S3 and S4). To elucidate these relationships, Pearson's correlation coefficients are calculated between wave attributes, ONI, and Atlantic TC count in Table 4. It is clear that there are strong, statistically significant correlations between AEW characteristics and ONI. AEW strength, mid- and low-level relative vorticity, and two measures of convective activity are all inversely correlated with ONI (R from -0.4 to -0.61) in both the ERA5 and MERRA-2 datasets.[2] Midlevel specific humidity around AEWs is also inversely correlated with ONI, though the correlation is weaker and only statistically significant for the ERA5 dataset. A negative correlation with ONI signifies that these values are elevated during La Niña conditions and reduced during El Niño conditions. This finding aligns with previous research using non-object-based identification methods that have shown a connection between AEW activity and ENSO phase (Ruti and Dell'Aquila 2010; Spinks and Lin 2015). Strong correlations with AEW

[2] Note that brightness temperatures T_b largely indicate cloud-top temperature, with lower values associated indicating more intense convection. Thus, the positive correlation shown for average T_b and ONI/TC count is indicative of a negative correlation between convective activity and these benchmarks.

Unauthenticated | Downloaded 10/23/26 03:43 PM UTC

TABLE 4. Pearson's correlation coefficients and associated p values between AEW characteristics in the Atlantic basin and either ONI or Atlantic TC count. Each variable is subset by the reanalysis dataset used. Correlations are bolded if they have a p value below 0.05. Captured TC genesis indicates the correlation between basinwide TC counts and the number of developing waves captured by the AEW tracker and is not calculated for the Atlantic TC counts.

		Correlations with ONI		Correlation with TC count	
Atlantic		R	p value	R	p value
AEW count	ERA5	−0.22	0.15	−0.29	0.06
	MERRA-2	−0.19	0.22	**−0.33**	**0.03**
AEW strength	ERA5	**−0.45**	**<0.01**	**0.39**	**0.01**
	MERRA-2	**−0.47**	**<0.01**	**0.31**	**0.04**
AEW latitude at 17.5°W	ERA5	0.00	0.99	−0.11	0.47
	MERRA-2	−0.07	0.64	−0.02	0.90
TC count	ERA5	**−0.41**	**0.01**	—	—
	MERRA-2	**−0.33**	**0.03**	—	—
400–700-hPa qv	ERA5	**−0.30**	**0.05**	**0.57**	**<0.01**
	MERRA-2	−0.29	0.06	**0.50**	**<0.01**
700–850-hPa qv	ERA5	−0.11	0.46	**0.52**	**<0.01**
	MERRA-2	−0.21	0.17	**0.51**	**<0.01**
400–700-hPa vorticity	ERA5	**−0.60**	**<0.01**	**0.42**	**<0.01**
	MERRA-2	**−0.61**	**<0.01**	**0.41**	**<0.01**
700–850-hPa vorticity	ERA5	**−0.59**	**<0.01**	**0.40**	**<0.01**
	MERRA-2	**−0.63**	**<0.01**	**0.38**	**0.01**
Average GridSat-B1 T_b	ERA5	**0.41**	**<0.01**	−0.28	0.07
	MERRA-2	**0.49**	**<0.01**	**−0.39**	**0.01**
Convective coverage	ERA5	**−0.40**	**<0.01**	**0.43**	**<0.01**
	MERRA-2	**−0.47**	**<0.01**	**0.49**	**<0.01**

attributes, including relative vorticity, moisture, and convective activity, further emphasize that this connection goes beyond AEW activity itself.

There is also an inverse correlation between the number of captured TC genesis cases from AEWs and the ONI. This is not surprising given the known connection between ENSO phase and TC activity in the Atlantic basin, where El Niño conditions reduce TC favorability through large-scale environmental changes (Shapiro 1987; Gray 1984; Landsea and Gray 1992; Aiyyer and Thorncroft 2006). It follows that many of the variables that are inversely correlated with the ONI are positively correlated with the Atlantic TC count (Table 4). Positive correlations indicate that years with increased Atlantic TC activity have AEWs that are stronger with enhanced near-wave-relative vorticity, moisture, and convection. This finding resembles previous research on intraseasonal time scales showing that AEW attributes—especially their lower-level circulation, convective coverage, and moisture content—can impact their favorability to undergo TC genesis (Hopsch et al. 2010; Brammer and Thorncroft 2015; Núñez Ocasio et al. 2021; Lawton and Majumdar 2023).

We also note the negative correlation between AEW count and TC count in the Atlantic basin. It is important to not overinterpret this finding given the uncertainties in the easterly wave count discussed in the previous section. Nevertheless, this could imply the increased importance of wave characteristics as opposed to total wave count in setting TC climatology. Indeed, recent modeling work has suggested that AEWs are not a limiting factor for TC genesis, instead emphasizing the role of environmental conditions surrounding TC seeds like easterly waves (Bercos-Hickey and Patricola 2023, 2025).

AEW-relative moisture, especially at low levels, appears much more correlated with the Atlantic TC count than ONI (Table 4). This may hint at the necessity of column moistening in the TC genesis process, as has been illustrated by previous research (Nolan 2007; Davis 2015). If AEWs are on average more humid in a given season, more waves could obtain the favorable moisture profiles necessary for TC genesis. There is also a negative correlation between AEW count and TC activity, though it is only significant in MERRA-2 data. This could partially be an artifact of the AEW tracker. Weaker AEWs may be more likely to drop below the tracking CV threshold and then "redevelop" as new waves, causing seasons with weaker average wave strength to have inflated wave counts. However, we caution against overinterpretation of this relationship given the uncertainty in the AEW count discussed in section 3.

We now shift to a more detailed analysis of these interannual AEW relationships and their regionality. In the following figures, AEWs are divided into waves that do undergo TC genesis ("developers") and those that do not ("nondevelopers"). We also use a discrete threshold for ONI (0.5) to separate El Niño and La Niña years and a percentage threshold (top and bottom 25%) to determine active and inactive Atlantic TC years. As discussed in section 2c, sensitivity testing was conducted for these thresholds and yielded similar results and conclusions (not shown). Results in this section generally complement the ONI and TC activity correlation measures shown in Table 4. It should also be reiterated that many of the active TC years overlap that of La Niña years (and vice versa for El Niño and inactive years), meaning results for these categories are not fully independent of one another and are thus expected to share similarities.

Unauthenticated | Downloaded 10/23/26 03:43 PM UTC

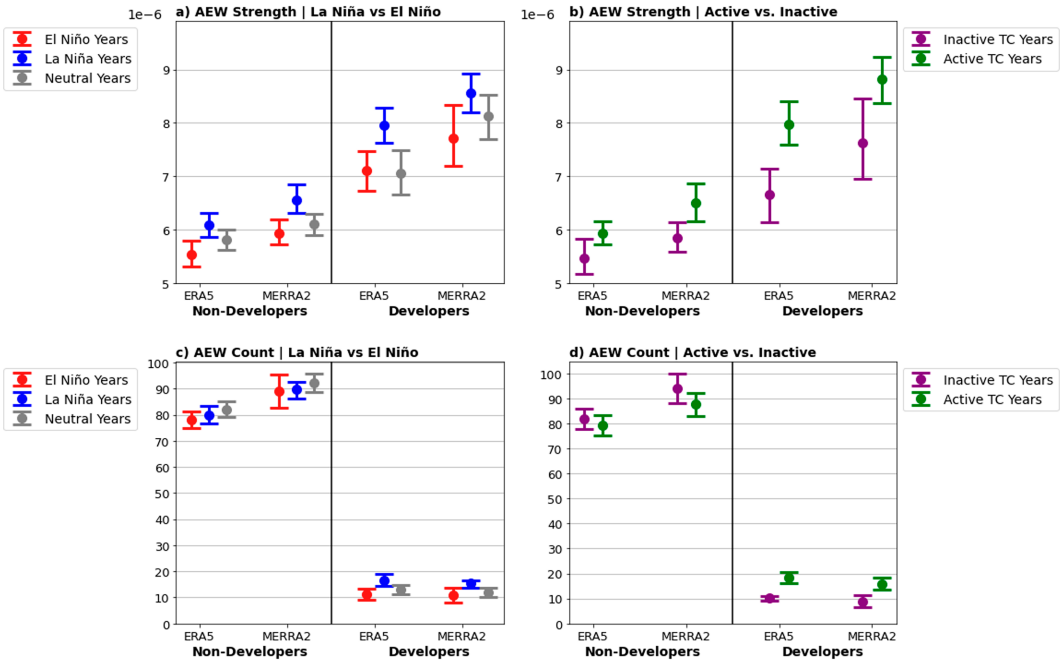


FIG. 6. Comparison of average (a),(b) AEW strength and (c),(d) total AEW count between (left) ENSO phases (red for El Niño; blue for La Niña; and gray for neutral) and (right) active/inactive TC years (purple for inactive and green for active). The data are subset into nondeveloping and developing AEWs, as well as the reanalysis dataset used to track and compute wave attributes. Circles indicate either (a),(b) the mean AEW strength or (c),(d) the total count. Whiskers encompass the 95% confidence interval via a bootstrapping technique.

A comparison of AEW count and strength between ENSO phases and active/inactive TC years is shown in Fig. 6. These results demonstrate a statistically significant increase in the average nondeveloping AEW strength in La Niña years as compared to El Niño years (Fig. 6a). Neutral year AEW strength is higher than during El Niño and lower than during La Niña, though only the La Niña–neutral year differences are statistically significant. A similar relationship exists for developing AEWs, but the limited sample size expands the confidence intervals and results in only the ERA5 dataset exceeding the 95% significance threshold. Nondeveloping AEW count is not significantly different between the ENSO phases (Fig. 6c). However, as expected, there are more developing AEWs in La Niña years than in El Niño and neutral years. AEWs also trend stronger during active TC years (Fig. 6b).

We also find that the association between AEW strength and ENSO phase is strongest over the continent of Africa. AEW strength is binned by longitude and compared between ENSO phases and active/inactive TC years in Fig. 7. Statistically significant differences in wave strength are generally confined

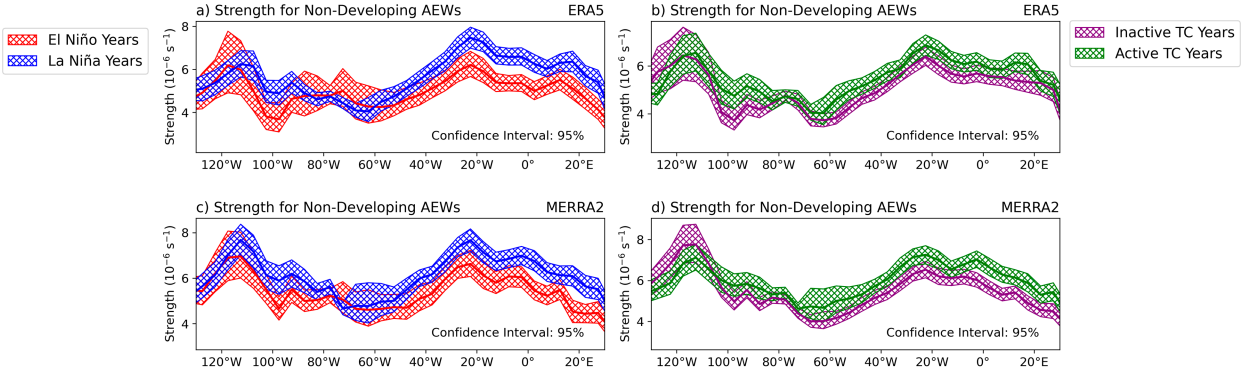


FIG. 7. Nondeveloping AEW strength binned by longitude for (a),(c) ENSO phases (red for El Niño and blue for La Niña) and (b),(d) active/inactive TC years (purple for inactive and green for active). Data are shown for (top) ERA5 and (bottom) MERRA-2. Values are binned every 5° longitude, with solid lines indicating the mean in each bin, and the hatched region depicts the 95% confidence interval using a bootstrapping technique. Longitude bins where hatched areas do not overlap are statistically significant.

Unauthenticated | Downloaded 10/23/26 03:43 PM UTC

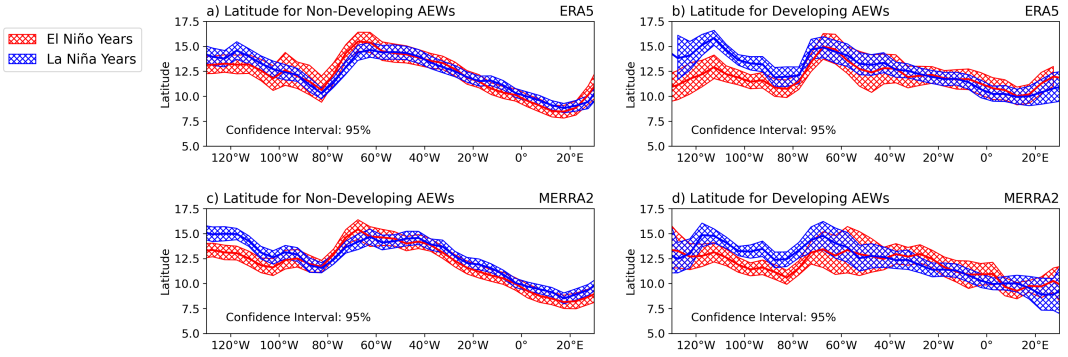


FIG. 8. (a),(c) As in Figs. 7a,c, but for the average latitude of AEWs in each longitude bin. (b),(d) As in (a) and (c), but for developing AEWs.

from 15°W to 20°E in both reanalyses, with AEWs strongest during La Niña years (Figs. 7a,c). ENSO differences persist west through 60°W, though the data over most of the eastern Atlantic is not statistically significant. A similar elevation in average wave strength is seen for active TC years over inactive years, though this is only statistically significant in MERRA-2 data over central Africa. Similar results are found for AEW strength between La Niña and neutral years, though the absolute differences are smaller in magnitude and the areas of statistical significance are less extensive (not shown).

Despite the clear relationship between AEW strength and ENSO phase, the same cannot be said for the latitude of nondeveloping AEWs (Fig. 8). No significant differences are seen with ENSO phase for AEW latitude over Africa and the Atlantic. Although the apparent lack of ENSO influence on latitude agrees with the Atlantic-wide correlations shown previously (Fig. 3e, Table 4), it is at odds with previous work indicating a northward shift in the AEJ–AEW system during La Niña (e.g., Spinks and Lin 2015). However, given the typical variability of the AEJ latitude within a given season and the large number of AEWs tracked each year, it is possible that such a relationship is obscured by noise.

In the eastern Pacific, meanwhile, there is a northward shift in easterly wave latitude during La Niña. This is especially true for developing AEWs. One hypothesis is that this pattern is a result of the unfavorability of the eastern Pacific to TC genesis during La Niña years, causing easterly waves that do become TCs to be preferentially located poleward from the equatorial region. ENSO is also known to shift the meridional location of the eastern Pacific intertropical convergence zone, which often migrates northward during La Niña years and could influence these waves (Rodrigues et al. 2011; Abe et al. 2014). As with AEW strength, a similar but less statistically significant pattern is found when comparing AEW latitude between La Niña and neutral years (not shown).

b. *AEW environmental characteristics*

Given the clear longitudinal dependence of the relationship between ENSO and AEW strength, it is expected that similar patterns exist for environmental variables surrounding tracked AEWs. Figure 9 depicts the difference between AEW-averaged relative vorticity and specific humidity in the vertical, as well as GridSat-B1 T_b, binned by longitude. While only ERA5 data are shown, results are similar for MERRA-2 composites and when comparing La Niña and neutral years (not shown). During La Niña years, midlevel (800–600 hPa) wave-relative vorticity is enhanced for nondeveloping easterly waves primarily over the African continent (20°W–30°E), with another region of enhancement in the Caribbean and eastern Pacific near Central America (Fig. 9a; 120°–80°W). Of particular note is the behavior of waves near the coastline of Africa where AEW circulations are known to climatologically deepen (Fig. 2a). There, differences in relative vorticity extend down to the lower troposphere. A similar pattern exists for AEW-relative specific humidity. Moisture is enhanced during La Niña years at midlevels over the African continent and at low levels over the eastern Atlantic and Caribbean (Fig. 9c). In contrast, easterly waves over the eastern Pacific appear weaker and drier during La Niña, reflecting their proximity to the ENSO region. Unlike nondeveloping AEWs, no widespread significant differences are found for developing AEWs.

Convective activity, meanwhile, is not statistically different across ENSO years for any individual longitude bin in the Atlantic. However, AEWs do trend slightly more convectively active (lower values of T_b) over the continent of Africa during La Niña (Fig. 9e). This may explain the basin-wide correlation between ONI and AEW-relative T_b shown in section 4a (Table 4). As with specific humidity and low-level relative vorticity, the convective activity around easterly waves in the eastern Pacific is reduced during La Niña.

Differences in AEW characteristics between active and inactive TC years largely follow the patterns found for ENSO and are shown in Fig. 10. Notably, differences in AEW-relative specific humidity are more prominent in this figure as compared to the ENSO figure, especially in the lower troposphere over the African continent. This aligns with the specific humidity correlations shown in Table 4, which were higher in magnitude and more likely to be statistically significant when correlated with the Atlantic TC activity as opposed to ONI.

These results further demonstrate a clear association between AEW characteristics—including wave strength, vertical structure, moisture content, and convective activity—and ENSO phase on interannual time scales. The highest magnitude and

Unauthenticated | Downloaded 10/23/26 03:43 PM UTC

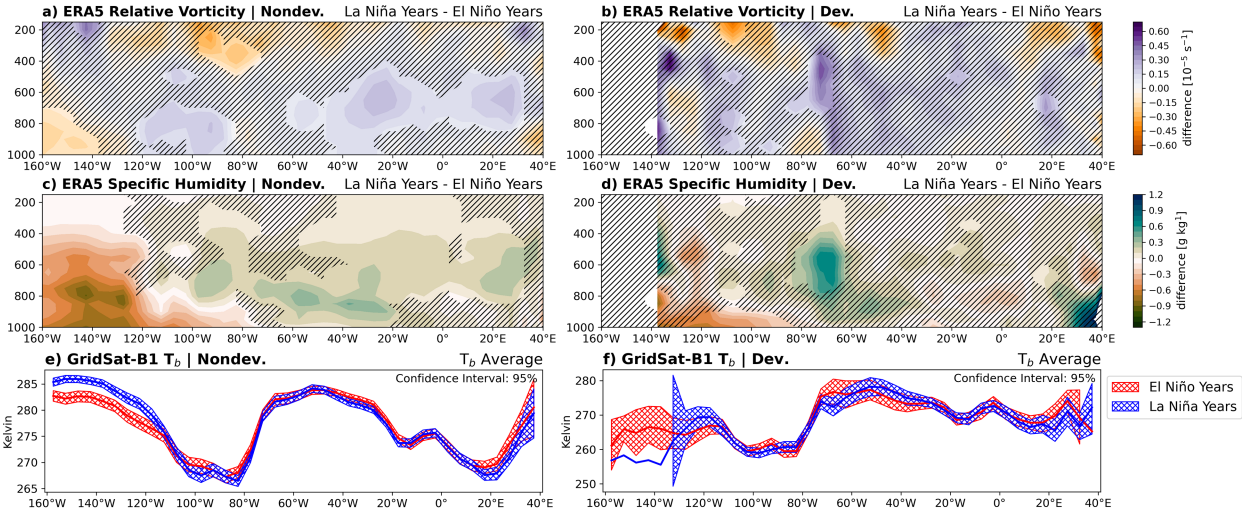


FIG. 9. As in Fig. 2, but showing instead the difference in vertical averages of (a),(b) AEW-averaged relative vorticity and (c),(d) specific humidity between La Niña and El Niño years in the ERA5 reanalysis dataset. Hatched regions are not statistically significantly different at a 95% threshold via a bootstrapping method. Data are subdivided into (left) nondeveloping and (right) developing AEWs. (e),(f) As in Fig. 7a, but computed for AEW-averaged GridSat-B1 T_b and divided into (e) nondeveloping and (f) developing AEWs.

most widespread changes occur when AEWs are located over Africa. This regionality hints at possible mechanisms connecting ENSO to AEWs through changes to local atmospheric circulations over Africa.

5. ENSO and atmospheric circulations over Africa

a. Basinwide characteristics

To better contextualize the interannual ENSO–AEW relationship explored in section 4, we now focus on atmospheric features over Africa during warm and cold ENSO phases and their potential influence on AEW characteristics. In particular, we highlight changes to the TEJ, AEJ, and the WAM, all three of which have had their interannual variability connected to ENSO in previous research (Janicot et al. 2001; Joly and Voldoire 2009; Spinks and Lin 2015; Vashisht et al. 2021; Didi et al. 2023). In this section, we limit basinwide averages to July–September instead of June–October, since these 3 months encompass the peak of AEW activity (Fig. 5). Note that unlike previous figures, dotted regions on these diagrams indicate that differences are significant at a 95% threshold.

Figure 11 illustrates average differences in these dynamic features between the La Niña and El Niño years used in our analysis. The TEJ is clearly much stronger and extends further west during La Niña years (Figs. 11a,b). This is important because previous work has shown that an enhanced TEJ is associated with reduced subsidence over the Sahel region and increased rainfall over central and eastern Africa (Grist and

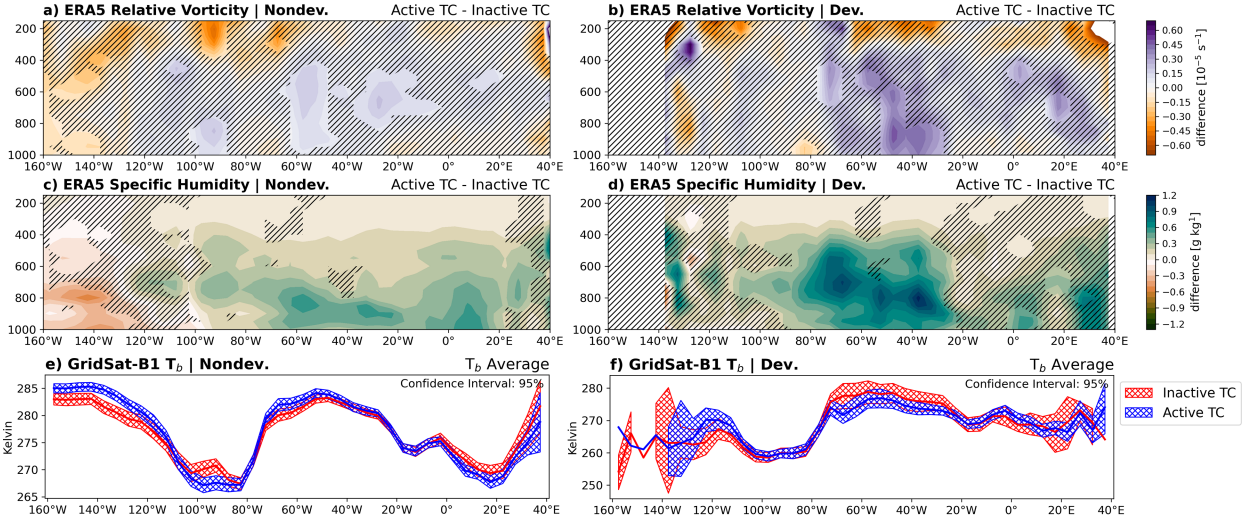


FIG. 10. As in Fig. 9, but for active–inactive TC years.

Unauthenticated | Downloaded 10/23/26 03:43 PM UTC

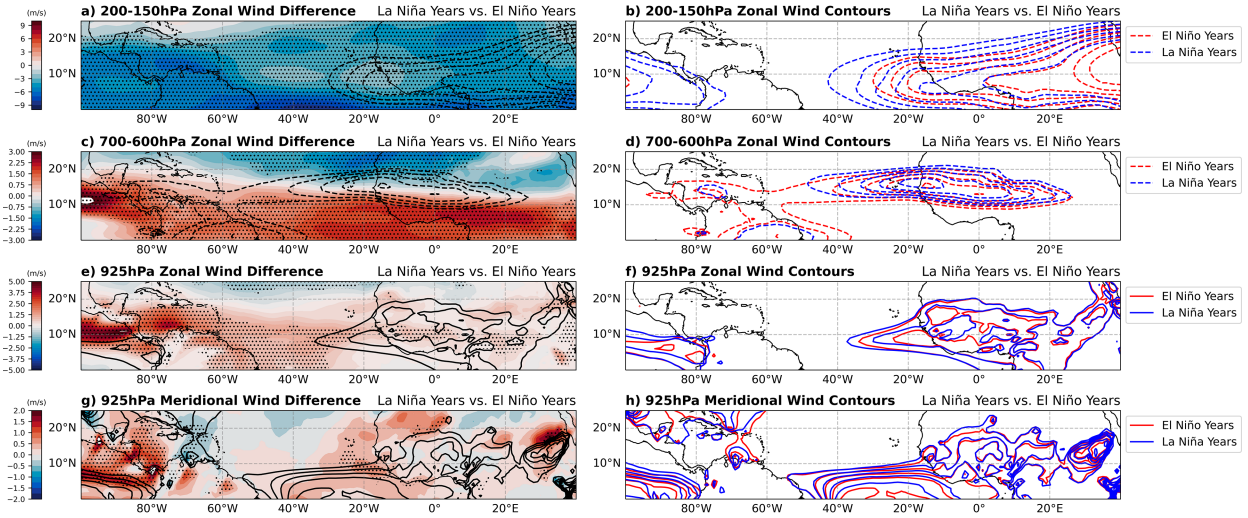


FIG. 11. The difference in the July–September average (a) 200–150-hPa zonal winds, (c) 700–600-hPa zonal winds, (e) 925-hPa zonal winds, and (g) 925-hPa meridional winds between La Niña years and El Niño years. Areas with statistically significant differences at a 95% threshold are hatched. (b),(d),(f),(h) Contours for El Niño (red) and La Niña (blue) years to better elucidate specific features over Africa. This includes (b) the TEJ (from −6 to −16 m s^{-1} at 2 m s^{-1} intervals), (d) the AEJ (from −7.5 to −11.5 m s^{-1} at 1 m s^{-1} intervals), (f) the zonal component of the WAM (1–10 m s^{-1} at 2 m s^{-1} intervals), and (h) the meridional component of the WAM (1–10 m s^{-1} at 2 m s^{-1} intervals).

Nicholson 2001; Gleixner et al. 2017; Vashisht et al. 2021). Meanwhile, the La Niña AEJ is shifted slightly poleward with a marginally increased wind maximum (Figs. 11c,d). A northward displacement of the AEJ has been associated with increased AEW activity and precipitation in West Africa (Sylla et al. 2010; Spinks and Lin 2015; Bercos-Hickey et al. 2020; Didi et al. 2023). It is also clear that the WAM circulation is much stronger in La Niña years as compared to El Niño years (Figs. 11g,h). A relationship between ENSO and WAM has also been noted in previous work and could be consequential since an enhanced WAM circulation can increase moisture advection and rainfall in the northern Sahel (Joly and Voldoire 2009).

Figures 12 and 13 show how these ENSO-related changes to circulation patterns affect vertical wind shear and moisture over Africa and the Atlantic. During La Niña years, deep-layer vertical wind shear is enhanced over most of central and West Africa, as well as the eastern Atlantic to about 40°W (Figs. 12a,b). This is primarily driven by changes to the TEJ (Figs. 11a,b). Low-level wind shear (600–925 hPa) increases in the northern Sahel (10°–20°N) and decreases south of this (from the equator to 10°N; Figs. 12c,d). Meanwhile, midlevel specific humidity is enhanced during La Niña years for most of continental Africa (Figs. 13a,b). Given the correspondence of these levels and latitudes with AEW activity (Fig. 1), the signal in midlevel specific humidity may be a result of the increased La Niña AEW activity itself. There is also a dipole in low-level humidity with increased values between 12° and 20°N and decreased values closer to the equator during La Niña (Figs. 13c,d). This is likely the result of the stronger WAM circulation.

b. *Potential connection to AEWs*

These basinwide patterns fit with previous theories and our own results connecting ENSO to interannual AEW variability. Ruti and Dell'Aquila (2010) argued that El Niño modifies large-scale subsidence over Africa. This subsidence is controlled in part by the TEJ. Additionally, Spinks and Lin (2015) suggested that the influence of ENSO on the TEJ can alter the strength of an east–west circulation cell that helps maintain the Saharan and Arabian highs. These highs help set the meridional

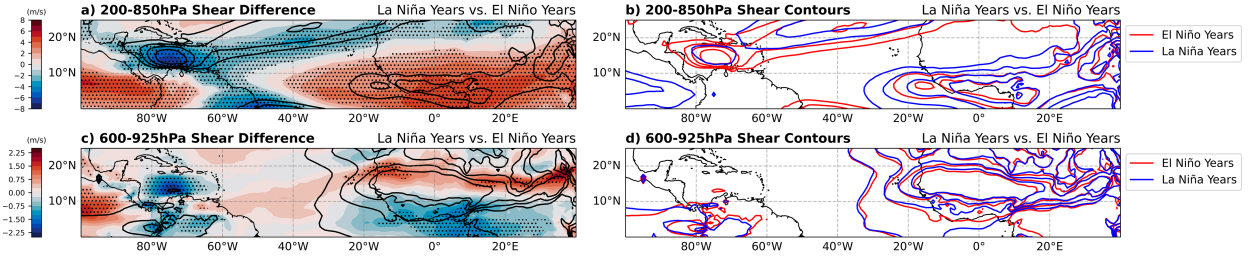


FIG. 12. As in Figs. 11a–d, but for the difference in (a),(b) 200–850-hPa vertical wind shear and (c),(d) 600–925-hPa vertical wind shear. The contours in (b) are spaced from 14 to 24 m s^{-1} at 2 m s^{-1} intervals, and those in (d) are spaced from 8 to 14 m s^{-1} at 2 m s^{-1} intervals.

Unauthenticated | Downloaded 10/23/26 03:43 PM UTC

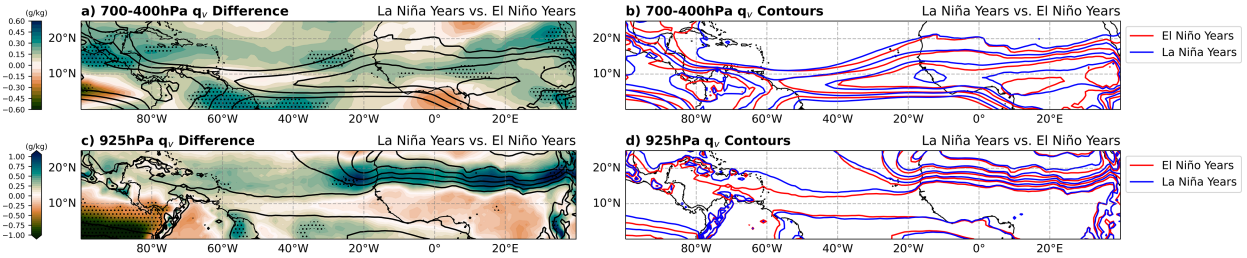


FIG. 13. As in Fig. 12, but for the difference in (a),(b) 700–400-hPa average specific humidity and (c),(d) 925-hPa specific humidity. The contours in (b) are spaced from 3 to 8 g kg^{-1} at 0.5 g kg^{-1} intervals, and those in (d) are spaced from 2 to 14 g kg^{-1} at 2 g kg^{-1} intervals.

temperature gradients that maintain the AEJ (Thorncroft and Blackburn 1999; Russell and Aiyyer 2020). We hypothesize that these changes drive a stronger TEJ (Figs. 11a,b) and a northward displacement of the AEJ (Figs. 11c,d) during La Niña years and are partially responsible for the increase in AEW strength, convective activity, and moisture that we show in section 4 (Figs. 6, 7, and 9). The influence on AEW activity could manifest, in part, through modifications to baroclinic and barotropic instabilities along the AEJ. However, as nearly 50% of AEW growth and propagation over the continent are driven by convective heating (Russell and Aiyyer 2020), the influence of the TEJ and AEJ on local wind shear, rainfall, and moisture could also help explain these differences (e.g., Figs. 7 and 9). Indeed, enhanced vertical wind shear over Africa, contributed to by regional circulation patterns, has been linked to long-lived MCSs with colder brightness temperatures and higher rain rates (Baidu et al. 2022).

Another potential factor that could link ENSO to interannual AEW variability is the WAM. A stronger WAM is associated with increased rainfall and moisture in the northern Sahel. Previous work has shown that a stronger WAM can provide the abundant moisture and wind shear necessary for the coupling of MCSs to AEWs, promoting their growth and encouraging downstream TC genesis (Núñez Ocasio et al. 2020, 2021). Thus, ENSO-driven changes to the WAM could also help explain the enhancements to AEW strength, moisture content, and convective activity we find during La Niña years (Figs. 6, 7, and 9).

Several caveats remain in our analysis. While we find an association between ENSO, the noted circulation patterns, and AEWs, this does not necessarily prove a cause-and-effect relationship. It is also difficult to disentangle the importance of individual factors and mechanisms using reanalysis data. Circulations over West and central Africa are closely coupled to one another, and changes to one aspect of the system are likely due to feedback on other aspects of the system (Nicholson 2013). We also note that slightly more La Niña years occurred in the modern era, which could be confounded by the observed climatological uptick in many wave-relative and basinwide environmental characteristics.

Despite these caveats, however, we note that we found a significant correlation between ENSO and AEW characteristics using a variety of methods and metrics. Such a relationship is supported by previous work into AEW activity and by the known impacts of ENSO on local circulation patterns. As a result, we argue that the totality of evidence presented here and in previous work strongly suggests that ENSO has an influence on AEW characteristics. These findings motivate future work on the connections between atmospheric circulations and AEWs using other tools, such as numerical models, which allow for causality to be more directly explored.

6. Conclusions and implications

a. *Summary*

Using an object-oriented AEW tracker, we examined the interannual variability of AEW characteristics and its association with ENSO and Atlantic TC activity. An analysis of tracked AEWs in two reanalysis datasets illustrated pronounced year-to-year variability in wave characteristics and their surrounding environmental fields. For most wave attributes, this variability was found to be well correlated between the reanalyses, implying the reliability of these fields as indicators of AEW activity. However, there are marked differences in seasonal AEW counts and the classification of "extreme" AEW years between datasets. This finding suggests that caution should be used when interpreting such statistics and that their utility in climatological studies may be limited. It is possible these differences are related to uncertainty in the reanalysis datasets, highlighting a need for future validation of reanalysis AEWs versus observations.

We found that ENSO significantly influences AEWs and their characteristics on interannual time scales, including their strength, moisture content, convective activity, and vertical structure. These AEW attributes are enhanced during La Niña years as compared to El Niño years. This relationship also appears to have a distinct regionality and is especially pronounced over the African continent. In contrast, easterly waves in the eastern Pacific generally exhibit an inverse relationship with ENSO as compared to Atlantic AEWs. While previous research has established a link between proxies for AEW activity and ENSO (Ruti and Dell'Aquila 2010; Spinks and Lin 2015; Dominguez et al. 2020), this is the first study to our knowledge that specifically describes the relationship between ENSO and AEW-following characteristics as well as its regionality. Furthermore, our utilization of tracked AEW objects differs from the indirect proxies for AEW activity used in previous studies and allows for individual wave features to be more directly quantified.

Because the strongest ENSO–AEW connections are located over the African continent, we hypothesize that several

Unauthenticated | Downloaded 10/23/26 03:43 PM UTC

regional circulations may link ENSO with interannual AEW behavior. For one, ENSO influences the TEJ over Africa, with a stronger and most extensive jet seen in La Niña years (Figs. 11a,b; shown previously by Vashisht et al. 2021). Additionally, the WAM is generally stronger and AEJ is displaced northward during La Niña years versus El Niño years (Figs. 11c–h; shown previously by Janicot et al. 2001; Spinks and Lin 2015). These circulation changes work together to increase low- and midlevel specific humidity, as well as to increase deep and shallow vertical wind shear, at the latitudes that AEWs typically propagate (Figs. 12 and 13). This may promote long-lived MCSs with increased rain rates that are more able to couple with propagating AEWs over Africa, increasing wave-relative moisture, convective activity, and growth (e.g., Núñez Ocasio et al. 2020, 2021; Baidu et al. 2022). Previous research has also suggested that increased TEJ strength during La Niña years may reduce large-scale subsidence and could indirectly enhance the meridional temperature gradients that drive the AEJ and its associated instabilities (Ruti and Dell'Aquila 2010; Spinks and Lin 2015). We note that while it is not possible to identify a dominant pathway or fully establish causality with the data presented here, previous research has shown that AEW growth and propagation are driven by both dynamic instabilities and diabatic heating from convective processes (Burpee 1972; Thorncroft and Hoskins 1994; Berry and Thorncroft 2012; Russell and Aiyyer 2020; Russell et al. 2020). Thus, we argue that ENSO-driven changes to the TEJ, AEJ, and WAM could influence wave dynamics through both of these growth mechanisms.

We also found that interannual AEW changes during active and inactive Atlantic TC years generally followed those shown for La Niña and El Niño years, albeit with a stronger relationship with mid- and low-level specific humidity than seen for ENSO (Table 4; Figs. 6, 7, and 10). On the one hand, this is not surprising given that these categories are not necessarily independent of one another (many of the ENSO and TC year selections used in this study overlap). Changes to large-scale atmospheric characteristics are known to increase Atlantic TC activity during La Niña years and reduce it during El Niño years. On the other hand, the similarity between AEW attributes in active TC/La Niña years (and vice versa) may suggest that ENSO influences seasonal AEW behavior in a way that affects TC genesis.

b. *ENSO–AEW modulation as a distinct TC teleconnection*

While ENSO has primarily been connected to Atlantic TC activity through its influence on vertical wind shear in the western Atlantic (Shapiro 1987; Aiyyer and Thorncroft 2006), there is reason to believe that the influence of ENSO on interannual AEW activity could be an additional teleconnection. Previous research has demonstrated that AEW characteristics over West and central Africa are predictive of their favorability to undergo TC genesis (Hopsch et al. 2010; Agudelo et al. 2011; Núñez Ocasio et al. 2021; Lawton and Majumdar 2023). For example, Lawton and Majumdar (2023) demonstrated that increased low-level relative vorticity, humidity, and convective coverage around AEWs over Africa increase their likelihood of TC genesis in the eastern Atlantic. Here, we show that similar AEW attributes were generally larger during La Niña years, including an enhancement of the full vertical circulation of AEWs as they left the coastline (Fig. 9a). This implies that a larger percentage of AEWs may obtain characteristics that make them favorable to TC genesis during La Niña years, potentially influencing Atlantic TC activity.

There are, however, some caveats to this interpretation. First, it is unclear how changes to the interannual distribution of AEW characteristics translate to individual AEW characteristics within a given season. It can be argued that marginal changes to individual AEWs are unlikely to impact their downstream favorability in a pronounced way. Another complication is that the increase in vertical wind shear over the African continent during La Niña, while potentially helpful for convective activity and MCS duration for AEWs over land, is likely to have a detrimental influence on TC genesis over the eastern Atlantic (Fig. 12). As such, it is unknown if ENSO-driven changes to AEWs can either 1) overcome detrimental vertical wind shear in the eastern Atlantic or 2) have an influence on TC genesis further downstream. Recent work has also questioned whether changes to AEW activity itself have as pronounced an impact on downstream TC genesis as previously suspected (Bercos-Hickey and Patricola 2025). These caveats illustrate the need for future research investigating the consequences of AEW variability on Atlantic TC activity.

c. *Other implications and future work*

Regardless of the impact it has on downstream TC activity, interannual fluctuations in AEW behavior have important impacts on rainfall, flooding, and drought in the African Sahel and Caribbean. AEWs also transport and interact with Saharan dust, which can travel across the Atlantic Ocean and reach locations in the Caribbean and Americas (Nathan et al. 2017; Burgess and Oyola-Merced 2024). As a result, the ENSO–AEW connection demonstrated in this study may have ramifications on seasonal forecasts and could indirectly affect other atmospheric phenomena. However, causal relationships are hard to disentangle from historical reanalysis data. We recommend follow-up work to address the mechanisms driving the ENSO–AEW connection noted here, especially using modeling frameworks where mechanisms can be more directly assessed. This would allow a more detailed analysis of ENSO-driven changes to the position and dynamics of circulation features like the TEJ and AEJ.

There also remains much uncertainty about the impact of global climate change on AEW activity (e.g., Akinsanola et al. 2025). In our analysis, we found an increasing trend in AEW strength, relative vorticity, and specific humidity across the 1981–2023 AEW climatology, though it was not significant using MERRA-2 data. We suggest the need for future research to better quantify how AEWs have changed in the observed record to better contextualize changes in future climate projections.

Acknowledgments. The authors wish to thank Dr. Phil Klotzbach and Dr. Emily Bercos-Hickey for helpful discussions

Unauthenticated | Downloaded 10/23/26 03:43 PM UTC

that greatly improved this work. We are also thankful for insightful feedback from NSF NCAR internal reviewer Dr. Falko Judt. Constructive comments from three anonymous reviewers also significantly improved this paper. The lead author acknowledges support from both an NSF Graduate Research Fellowship (1938060) and an NCAR ASP Postdoctoral Fellowship while conducting this research. This material is based upon work supported by the National Center for Atmospheric Research, which is a major facility sponsored by the National Science Foundation under Cooperative Agreement 1852977. The second and third authors acknowledge support from NSF Grants AGS-1747781 and AGS-2438140.

Data availability statement. AEW tracks used in this study were generated via the QTrack Python module v0.0.4, first developed by Lawton et al. (2022), which is available on GitHub (Lawton 2024a; https://github.com/qlawton/QTrack). These historical tracks are also published in an online repository (Lawton 2024b; https://doi.org/10.5281/zenodo.13350859). ERA5 data were obtained via the Copernicus Climate Data Store at http://cds.climate.copernicus.eu (Hersbach et al. 2020). MERRA-2 data were obtained via NASA's GES-DISC at https://disc.gsfc.nasa.gov/datasets?project=MERRA-2 (Gelaro et al. 2017). GridSat-B1 satellite data were obtained from https://www.ncdc.noaa.gov/gridsat/gridsat-index.php (Knapp et al. 2011).

REFERENCES

Abe, H., Y. Tanimoto, T. Hasegawa, N. Ebuchi, and K. Hanawa, 2014: Oceanic Rossby waves induced by the meridional shift of the ITCZ in association with ENSO events. *J. Oceanogr.*, **70**, 165–174, https://doi.org/10.1007/s10872-014-0220-1.

Aiyyer, A. R., and C. Thorncroft, 2006: Climatology of vertical wind shear over the tropical Atlantic. *J. Climate*, **19**, 2969–2983, https://doi.org/10.1175/JCLI3685.1.

Akinsanola, A. A., A. A. Adebiyi, V. Bobde, O. E. Adeyeri, A. T. Tamoff, and D. K. Danso, 2025: Projected changes in African easterly wave activity due to climate change. *Commun. Earth Environ.*, **6**, 2, https://doi.org/10.1038/s43247-024-01981-9.

Alaka, G. J., Jr., and E. D. Maloney, 2012: The influence of the MJO on upstream precursors to African easterly waves. *J. Climate*, **25**, 3219–3236, https://doi.org/10.1175/JCLI-D-11-00232.1.

——, and ——, 2014: The intraseasonal variability of African easterly wave energetics. *J. Climate*, **27**, 6559–6580, https://doi.org/10.1175/JCLI-D-14-00146.1.

Agudelo, P. A., C. D. Hoyos, J. A. Curry, and P. J. Webster, 2011: Probabilistic discrimination between large-scale environments of intensifying and decaying African easterly waves. *Climate Dyn.*, **36**, 1379–1401, https://doi.org/10.1007/s00382-010-0851-x.

Baidu, M., J. Schwendike, J. H. Marshan, and C. Bain, 2022: Effects of vertical wind shear on intensities of mesoscale convective systems over west and central Africa. *Atmos. Sci. Lett.*, **23**, e1094, https://doi.org/10.1002/asl.1094.

Bain, C. L., K. D. Williams, S. F. Milton, and J. T. Heming, 2014: Objective tracking of African easterly waves in Met Office models. *Quart. J. Roy. Meteor. Soc.*, **140**, 47–57, https://doi.org/10.1002/qj.2110.

Belanger, J. I., M. T. Jelinek, and J. A. Curry, 2016: A climatology of easterly waves in the tropical Western Hemisphere. *Geosci. Data J.*, **3**, 40–49, https://doi.org/10.1002/gdj3.40.

Bercos-Hickey, E., and C. M. Patricola, 2023: The effects of African easterly wave suppression by wave track on Atlantic tropical cyclones. *Geophys. Res. Lett.*, **50**, e2023GL105491, https://doi.org/10.1029/2023GL105491.

——, and ——, 2024: African easterly wave strength and observed Atlantic tropical cyclone genesis and characteristics. *J. Geophys. Res. Atmos.*, **129**, e2024JD040858, https://doi.org/10.1029/2024JD040858.

——, and ——, 2025: Drivers of Atlantic tropical cyclogenesis: African easterly waves and the environment. *Geophys. Res. Lett.*, **52**, e2024GL112002, https://doi.org/10.1029/2024GL112002.

——, T. R. Nathan, and S.-H. Chen, 2020: On the relationship between the African easterly jet, Saharan mineral dust aerosols, and West African precipitation. *J. Climate*, **33**, 3533–3546, https://doi.org/10.1175/JCLI-D-18-0661.1.

Berry, G. J., and C. D. Thorncroft, 2012: African easterly wave dynamics in a mesoscale numerical model: The upscale role of convection. *J. Atmos. Sci.*, **69**, 1267–1283, https://doi.org/10.1175/JAS-D-11-099.1.

Brammer, A., and C. D. Thorncroft, 2015: Variability and evolution of African easterly wave structures and their relationship with tropical cyclogenesis over the eastern Atlantic. *Mon. Wea. Rev.*, **143**, 4975–4995, https://doi.org/10.1175/MWR-D-15-0106.1.

——, and ——, 2017: Spatial and temporal variability of the three-dimensional flow around African easterly waves. *Mon. Wea. Rev.*, **145**, 2879–2895, https://doi.org/10.1175/MWR-D-16-0454.1.

Burgess, R. W., and M. I. Oyola-Merced, 2024: Saharan dust impact on radiative heating rate errors inherent in reanalysis data in the African easterly wave development region. *Atmos. Chem. Phys.*, **24**, 12 183–12 201, https://doi.org/10.5194/acp-24-12183-2024.

Burpee, R. W., 1972: The origin and structure of easterly waves in the lower troposphere of North Africa. *J. Atmos. Sci.*, **29**, 77–90, https://doi.org/10.1175/1520-0469(1972)029<0077:TOASOE>2.0.CO;2.

Camargo, S. J., K. A. Emanuel, and A. H. Sobel, 2007: Use of a genesis potential index to diagnose ENSO effects on tropical cyclone genesis. *J. Climate*, **20**, 4819–4834, https://doi.org/10.1175/JCLI4282.1.

Cornforth, R. J., B. J. Hoskins, and C. D. Thorncroft, 2009: The impact of moist processes on the African easterly jet–African easterly wave system. *Quart. J. Roy. Meteor. Soc.*, **135**, 894–913, https://doi.org/10.1002/qj.414.

Davis, C. A., 2015: The formation of moist vortices and tropical cyclones in idealized simulations. *J. Atmos. Sci.*, **72**, 3499–3516, https://doi.org/10.1175/JAS-D-15-0027.1.

Didi, S. R., M. Diakhaté, and A. Diedhiou, 2023: Changes in the West Africa monsoon precipitation extremes during ENSO developing phases. *Atmos.–Ocean*, **61**, 293–305, https://doi.org/10.1080/07055900.2023.2202656.

Dominguez, C., J. M. Done, and C. L. Bruyère, 2020: Easterly wave contributions to seasonal rainfall over the tropical Americas in observations and a regional climate model. *Climate Dyn.*, **54**, 191–209, https://doi.org/10.1007/s00382-019-04996-7.

Downs, W. B., S. J. Majumdar, and A. D. Mahoney, 2025: Using deep learning to identify tropical easterly waves, the intertropical convergence zone, and the monsoon trough. *Mon. Wea. Rev.*, **153**, 1581–1604.

Unauthenticated | Downloaded 10/23/26 03:43 PM UTC

Fischer, C., A. H. Fink, E. Schömer, M. Rautenhaus, and M. Riemer, 2024: An objective identification technique for potential vorticity structures associated with African easterly waves. *Geosci. Model Dev.*, **17**, 4213–4228, https://doi.org/10.5194/gmd-17-4213-2024.

Gelaro, R., and Coauthors, 2017: The Modern-Era Retrospective Analysis for Research and Applications, version 2 (MERRA-2). *J. Climate*, **30**, 5419–5454, https://doi.org/10.1175/JCLI-D-16-0758.1.

Gleixner, S., N. Keenlyside, E. Viste, and D. Korecha, 2017: The El Niño effect on Ethiopian summer rainfall. *Climate Dyn.*, **49**, 1865–1883, https://doi.org/10.1007/s00382-016-3421-z.

Gray, W. M., 1984: Atlantic seasonal hurricane frequency. Part I: El Niño and 30 mb quasi-biennial oscillation influences. *Mon. Wea. Rev.*, **112**, 1649–1668, https://doi.org/10.1175/1520-0493(1984)112<1649:ASHFPI>2.0.CO;2.

Grist, J. P., and S. E. Nicholson, 2001: A study of the dynamic factors influencing the rainfall variability in the West African Sahel. *J. Climate*, **14**, 1337–1359, https://doi.org/10.1175/1520-0442(2001)014<1337:ASOTDF>2.0.CO;2.

Hall, N. M. J., G. N. Kiladis, and C. D. Thorncroft, 2006: Three-dimensional structure and dynamics of African easterly waves. Part II: Dynamical modes. *J. Atmos. Sci.*, **63**, 2231–2245, https://doi.org/10.1175/JAS3742.1.

Hannah, W. M., and A. Aiyyer, 2017: Reduced African easterly wave activity with quadrupled CO_2 in the superparameterized CESM. *J. Climate*, **30**, 8253–8274, https://doi.org/10.1175/JCLI-D-16-0822.1.

Hersbach, H., and Coauthors, 2020: The ERA5 global reanalysis. *Quart. J. Roy. Meteor. Soc.*, **146**, 1999–2049, https://doi.org/10.1002/qj.3803.

Hollis, M. A., R. R. McCrary, J. P. Stachnik, C. Lewis-Merritt, and E. R. Martin, 2024: A global climatology of tropical easterly waves. *Climate Dyn.*, **62**, 2317–2332, https://doi.org/10.1007/s00382-023-07025-w.

Hopsch, S. B., C. D. Thorncroft, and K. R. Tyle, 2010: Analysis of African easterly wave structures and their role in influencing tropical cyclogenesis. *Mon. Wea. Rev.*, **138**, 1399–1419, https://doi.org/10.1175/2009MWR2760.1.

Hsieh, J.-S., and K. H. Cook, 2005: Generation of African easterly wave disturbances: Relationship to the African easterly jet. *Mon. Wea. Rev.*, **133**, 1311–1327, https://doi.org/10.1175/MWR2916.1.

——, and ——, 2007: A study of the energetics of African easterly waves using a regional climate model. *J. Atmos. Sci.*, **64**, 421–440, https://doi.org/10.1175/JAS3851.1.

Janicot, S., S. Trzaska, and I. Poccard, 2001: Summer Sahel-ENSO teleconnection and decadal time scale SST variations. *Climate Dyn.*, **18**, 303–320, https://doi.org/10.1007/s003820100172.

Janiga, M. A., and C. D. Thorncroft, 2013: Regional differences in the kinematic and thermodynamic structure of African easterly waves. *Quart. J. Roy. Meteor. Soc.*, **139**, 1598–1614, https://doi.org/10.1002/qj.2047.

Johnston, B. R., W. J. Randel, and J. P. Sjoberg, 2021: Evaluation of tropospheric moisture characteristics among COSMIC-2, ERA5 and MERRA-2 in the tropics and subtropics. *Remote Sens.*, **13**, 880, https://doi.org/10.3390/rs13050880.

Joly, M., and A. Voldoire, 2009: Influence of ENSO on the West African monsoon: Temporal aspects and atmospheric processes. *J. Climate*, **22**, 3193–3210, https://doi.org/10.1175/2008JCLI2450.1.

Kim, D., S. K. Lee, H. Lopez, G. R. Foltz, C. Wen, R. West, and J. Dunion, 2023: Increase in Cape Verde hurricanes during Atlantic Niño. *Nat. Commun.*, **14**, 3704, https://doi.org/10.1038/s41467-023-39467-5.

Knapp, K. R., and Coauthors, 2011: Globally gridded satellite observations for climate studies. *Bull. Amer. Meteor. Soc.*, **92**, 893–907, https://doi.org/10.1175/2011BAMS3039.1.

Landsea, C. W., 1993: A climatology of intense (or major) Atlantic hurricanes. *Mon. Wea. Rev.*, **121**, 1703–1713, https://doi.org/10.1175/1520-0493(1993)121<1703:ACOIMA>2.0.CO;2.

——, and W. M. Gray, 1992: The strong association between western Sahelian monsoon rainfall and intense Atlantic hurricanes. *J. Climate*, **5**, 435–453, https://doi.org/10.1175/1520-0442(1992)005<0435:TSABWS>2.0.CO;2.

——, and J. L. Franklin, 2013: Atlantic hurricane database uncertainty and presentation of a new database format. *Mon. Wea. Rev.*, **141**, 3576–3592, https://doi.org/10.1175/MWR-D-12-00254.1.

Lawton, Q. A., 2024a: QTrack (version v0.0.4): An African easterly wave tracker. Accessed 20 August 2024, https://github.com/qlawton/QTrack.

——, 2024b: Objective African easterly tracks in reanalysis data using "QTrack". Zenodo, accessed 20 August 2024, https://doi.org/10.5281/zenodo.14338645.

——, and S. J. Majumdar, 2023: Convectively coupled kelvin waves and tropical cyclogenesis: Connections through convection and moisture. *Mon. Wea. Rev.*, **151**, 1647–1666, https://doi.org/10.1175/MWR-D-23-0005.1.

——, ——, K. Dotterer, C. Thorncroft, and C. J. Schreck III, 2022: The influence of convectively coupled kelvin waves on African easterly waves in a wave-following framework. *Mon. Wea. Rev.*, **150**, 2055–2072, https://doi.org/10.1175/MWR-D-21-0321.1.

Leroux, S., and N. M. J. Hall, 2009: On the relationship between African easterly waves and the African easterly jet. *J. Atmos. Sci.*, **66**, 2303–2316, https://doi.org/10.1175/2009JAS2988.1.

Lubis, S. W., and C. Jacobi, 2015: The modulating influence of Convectively Coupled Equatorial Waves (CCEWs) on the variability of tropical precipitation. *Int. J. Climatol.*, **35**, 1465–1483, https://doi.org/10.1002/joc.4069.

Nathan, T. R., D. F. P. Grogan, and S.-H. Chen, 2017: Subcritical destabilization of African easterly waves by Saharan mineral dust. *J. Atmos. Sci.*, **74**, 1039–1055, https://doi.org/10.1175/JAS-D-16-0247.1.

Nicholson, S. E., 2013: The West African Sahel: A review of recent studies on the rainfall regime and its interannual variability. *Int. Scholarly Res. Not.*, **2013**, 453521, https://doi.org/10.1155/2013/453521.

NOAA, 2009: Climate variability: Oceanic Niño Index. Accessed 15 October 2023, https://www.climate.gov/news-features/understanding-climate/climate-variability-oceanic-nino-index.

Nolan, D. S., 2007: What is the trigger for tropical cyclogenesis? *Aust. Meteor. Mag.*, **56**, 241–266.

Núñez Ocasio, K. M., J. L. Evans, and G. S. Young, 2020: A wave-relative framework analysis of AEW–MCS interactions leading to tropical cyclogenesis. *Mon. Wea. Rev.*, **148**, 4657–4671, https://doi.org/10.1175/MWR-D-20-0152.1.

——, A. Brammer, J. L. Evans, G. S. Young, and Z. L. Moon, 2021: Favorable monsoon environment over eastern Africa for subsequent tropical cyclogenesis of African easterly waves. *J. Atmos. Sci.*, **78**, 2911–2925, https://doi.org/10.1175/JAS-D-20-0339.1.

——, C. A. Davis, Z. L. Moon, and Q. A. Lawton, 2024: Moisture dependence of an african easterly wave within the West African

Unauthenticated | Downloaded 10/23/26 03:43 PM UTC

monsoon system. *J. Adv. Model. Earth Syst.*, **16**, e2023MS004070, https://doi.org/10.1029/2023MS004070.

Patricola, C. M., R. Saravanan, and P. Chang, 2014: The impact of the El Niño–Southern Oscillation and Atlantic meridional mode on seasonal Atlantic tropical cyclone activity. *J. Climate*, **27**, 5311–5328, https://doi.org/10.1175/JCLI-D-13-00687.1.

Prein, A. F., and Coauthors, 2024: Km-scale simulations of mesoscale convective systems over South America—A feature tracker intercomparison. *J. Geophys. Res. Atmos.*, **129**, e2023JD040254, https://doi.org/10.1029/2023JD040254.

Rodrigues, R. R., R. J. Haarsma, E. J. D. Camps, and T. Ambrizzi, 2011: The impacts of inter–El Niño variability on the tropical Atlantic and northeast Brazil climate. *J. Climate*, **24**, 3402–3422, https://doi.org/10.1175/2011JCLI3983.1.

Russell, J. O., A. Aiyyer, J. D. White, and W. Hannah, 2017: Revisiting the connection between African easterly waves and Atlantic tropical cyclogenesis. *Geophys. Res. Lett.*, **44**, 587–595, https://doi.org/10.1002/2016GL071236.

Russell, J. O. H., and A. Aiyyer, 2020: The potential vorticity structure and dynamics of African easterly waves. *J. Atmos. Sci.*, **77**, 871–890, https://doi.org/10.1175/JAS-D-19-0019.1.

——, ——, and J. D. White, 2020: African easterly wave dynamics in convection-permitting simulations: Rotational stratiform instability as a conceptual model. *J. Adv. Model. Earth Syst.*, **12**, e2019MS001706, https://doi.org/10.1029/2019MS001706.

Ruti, P. M., and A. Dell'Aquila, 2010: The twentieth century African easterly waves in reanalysis systems and IPCC simulations, from intra-seasonal to inter-annual variability. *Climate Dyn.*, **35**, 1099–1117, https://doi.org/10.1007/s00382-010-0894-z.

Shapiro, L. J., 1987: Month-to-month variability of the Atlantic tropical circulation and its relationship to tropical storm formation. *Mon. Wea. Rev.*, **115**, 2598–2614, https://doi.org/10.1175/1520-0493(1987)115<2598:MTMVOT>2.0.CO;2.

Skinner, C. B., and N. S. Diffenbaugh, 2014: Projected changes in African easterly wave intensity and track in response to greenhouse forcing. *Proc. Natl., Acad. Sci.*, **111**, 6882–6887, https://doi.org/10.1073/pnas.1319597111.

Spinks, J. D., and Y.-L. Lin, 2015: Variability of the subtropical highs, African easterly jet and easterly wave intensities over North Africa and Arabian Peninsula in late summer. *Int. J. Climatol.*, **35**, 3540–3555, https://doi.org/10.1002/joc.4226.

Sultan, B., S. Janicot, and A. Diedhiou, 2003: The West African monsoon dynamics. Part I: Documentation of intraseasonal variability. *J. Climate*, **16**, 3389–3406, https://doi.org/10.1175/1520-0442(2003)016<3389:TWAMDP>2.0.CO;2.

Sylla, M. B., A. Dell'Aquila, P. M. Ruti, and F. Giorgi, 2010: Simulation of the intraseasonal and the interannual variability of rainfall over west Africa with RegCM3 during the monsoon period. *Int. J. Climatol.*, **30**, 1865–1883, https://doi.org/10.1002/joc.2029.

Thorncroft, C. D., and B. J. Hoskins, 1994: An idealized study of African easterly waves. I: A linear view. *Quart. J. Roy. Meteor. Soc.*, **120**, 953–982, https://doi.org/10.1002/qj.49712051809.

——, and M. Blackburn, 1999: Maintenance of the African easterly jet. *Quart. J. Roy. Meteor. Soc.*, **125**, 763–786, https://doi.org/10.1002/qj.49712555502.

——, and K. Hodges, 2001: African easterly wave variability and its relationship to Atlantic tropical cyclone activity. *J. Climate*, **14**, 1166–1179, https://doi.org/10.1175/1520-0442(2001)014<1166:AEWVAI>2.0.CO;2.

——, N. M. J. Hall, and G. N. Kiladis, 2008: Three-dimensional structure and dynamics of African easterly waves. Part III: Genesis. *J. Atmos. Sci.*, **65**, 3596–3607, https://doi.org/10.1175/2008JAS2575.1.

Tomassini, L., 2018: Mesoscale circulations and organized convection in African easterly waves. *J. Atmos. Sci.*, **75**, 4357–4381, https://doi.org/10.1175/JAS-D-18-0183.1.

Torres, V. M., C. D. Thorncroft, and N. M. J. Hall, 2021: Genesis of easterly waves over the tropical eastern Pacific and the intra-Americas sea. *J. Atmos. Sci.*, **78**, 3263–3279, https://doi.org/10.1175/JAS-D-20-0389.1.

Vargas Martes, R. M., Á. F. Adames Corraliza, and V. C. Mayta, 2023: The role of water vapor and temperature in the thermodynamics of tropical northeast Pacific and African easterly waves. *J. Atmos. Sci.*, **80**, 2305–2322, https://doi.org/10.1175/JAS-D-22-0177.1.

Vashisht, A., B. Zaitchik, and A. Gnanadesikan, 2021: ENSO teleconnection to eastern African summer rainfall in global climate models: Role of the tropical easterly jet. *J. Climate*, **34**, 293–312, https://doi.org/10.1175/JCLI-D-20-0222.1.

Vecchi, G. A., C. Landsea, W. Zhang, G. Villarini, and T. Knutson, 2021: Changes in Atlantic major hurricane frequency since the late-19th century. *Nat. Commun.*, **12**, 4054, https://doi.org/10.1038/s41467-021-24268-5.

Ventrice, M. J., and C. D. Thorncroft, 2013: The role of convectively coupled atmospheric Kelvin waves on African easterly wave activity. *Mon. Wea. Rev.*, **141**, 1910–1924, https://doi.org/10.1175/MWR-D-12-00147.1.

Zhou, Y., and E. D. Maloney, 2025: Dynamics and energetics associated with two East Pacific easterly waves during the OTREC campaign in August 2019. *J. Geophys. Res. Atmos.*, **130**, e2024JD042266, https://doi.org/10.1029/2024JD042266.

Unauthenticated | Downloaded 10/23/26 03:43 PM UTC